SILICON AND CARBON BASED NANOWIRES

A THESIS

SUBMITTED TO THE DEPARTMENT OF PHYSICS

AND THE INSTITUTE OF ENGINEERING AND SCIENCE

OF BİLKENT UNIVERSITY

IN PARTIAL FULFILLMENT OF THE REQUIREMENTS

FOR THE DEGREE OF

MASTER OF SCIENCE

By

Sefaattin TONGAY

January, 2004

I certify that I have read this thesis and that in my opinion it is fully adequate, in scope and in quality, as a thesis for the degree of Master of Science.

Prof. Dr. Salim Çıracı (Advisor)

I certify that I have read this thesis and that in my opinion it is fully adequate, in scope and in quality, as a thesis for the degree of Master of Science.

Prof. Dr. Atilla Aydınlı

I certify that I have read this thesis and that in my opinion it is fully adequate, in scope and in quality, as a thesis for the degree of Master of Science.

Prof. Dr. Şakir Erkoç

Approved for the Institute of Engineering and Science:

Prof. Dr. Mehmet B. Baray
Director of the Institute Engineering and Science

ABSTRACT

SILICON AND CARBON BASED NANOWIRES

Sefaattin TONGAY
M.S. in Physics
Supervisor: Prof. Dr. Salim Çıracı
January, 2004

Nanowires have been an active field of study since last decade. The reduced dimensionality end size allowing electrons can propagate only in one direction has led to quantization which are rather different from the bulk structure. As a result, nanowires having cross section in the range of Broglie wavelength have shown stepwise electrical and thermal conductance, giant Young modulus, stepwise variation of the cross-section etc. Moreover, the atomic structure of nanowires have exhibited interesting regularities which are not known in two or three dimensions. These novel properties of nanowires have been actively explored since last decade in order to find an application in the rapidly developing field of nanotechnology.

In the present thesis, we investigated the atomic and electronic structure of a variety of Si and C atom based very thin nanowires starting from linear chain including pentagonal, hexagonal and tubular structures. We found that the C and Si linear chains form double bonds and have high binding energy. Although bulk carbon in diamond structure is an insulator, carbon linear chain is metal and has twice conductance of the gold chain. We carried out an extensive analysis of stability and conductance of the other wires. Our study reveals that Si and C based nanowires generally show metallic properties in spite of the fact that they are insulator or semiconductor when they are in bulk crystal structure. Metallicity occurs due to change in the character and order of bonds.

Keywords: ab initio, first principles, nanowires, density functional theory, nanotubes, conductance.

ÖZET

SİLİKON VE KARBON TABANLI NANOTELLER

Sefaattin TONGAY
Fizik , Yüksek Lisans
Tez Yöneticisi: Prof. Dr. Salim Çıracı
Ocak, 2004

Nanoteller geçen on yıldan beridir aktif bir araştırma alanidir. İndirgenmiş boyut ve büyüklügün elektronların bir yönlü hareketine izin vermesi, bulk yapıdan oldukça farklı olarak, kesikliliğe sebebiyet vermektedir. Sonuç olarak, Broglie dalgaboyu mertebesinde kesit alanına sahip nanoteller, basamaklı yapıda elektriksel ve ısısal iletkenlik, yüksek Young modulü ve kesikli olarak değişen kesit alanı gibi özellikler göstermektedir. Dahası, nanotellerin atomik yapısı iki ve üç boyutta bilinmeyen ilginç düzenliliğe sahiptir. Nanotellerin bu belli başlı özellikleri nanoteklonojinin hızla gelişen alanlarında bir uygulama bulmak amacıyla geçtigimiz on yıldan beridir aktif olarak araştırılmaktadır.

Bu tezde, silikon ve karbon içn doğrusal zincir yapıdan başlayarak, beşgensel, altıgensel ve tüpsel yapıların atomik ve elektronik yapılari incelenmiştir. C ve Si doğrusal zincir yapılarında çift bağ oluşumu sebebiyle bu yapıların yüksek bağlanma enerjisine sahip oldukları bulunmuştur. Elmas yapıdaki bulk karbon yalıtkan olmakla beraber, karbon doğrusal zincir yapı metalik olup, altın doğrusal zincir yapıya nazaran iki kat iletkenliğe sahiptir. Diğer tel yapılar icin detaylı kararlılık ve iletkenlik analizleri yürütülmüştür. Yapılan analizler Si ve C temelli nanotellerin, bulk kristal yapılarının yalıtkan veya yarıiletken olmasına rağmen, genel olarak metalik özelliklere sahip olduğunu göstermektedir. Bu metalik davranış, bağların karekterindeki ve yönlenimindeki değişiklikten ileri gelmektedir.

Anahtar sözcükler: ab initio, temel prensipler, nanoteller, durum fonksiyonu teorisi, karbon nanotüp, iletkenlik.

Acknowledgement

I would like to express my deepest gratitude and respect to my supervisor Prof. Dr. Salim Çıracı for his patience and guidance during my study including nights and weekends and also for giving me a chance to be one his assistant. I really feel lucky to meet him...

I am thankful to Assc. Prof. Dr. Oğuz Gülseren and Dr. Tuğrul Senger for his valuable discussions and advices.

I appreciate Prof. Dr. Atilla Aydınlı for his motivation. I'm very glad to be one his assistant in freshmen physics course for three semesters.

I also remember Prof. Dr. Hüseyin Erbil, Prof. Dr. Nizamettin Armağan whose discussions and thoughts have always motivated me and give very valuable physical interpretation, my senior project advisor Prof. Dr. Emine Cebe and Prof. Dr. Fevzi Büyükkilinç for the days I spent in Ege University theoretical physics department.

My sincere thanks due to Dr. Ceyhun Bulutay for his motivation and guidance but especially for the human profile he draws which I imagine to be like one in future.

I would like to thank to my companion, my home-mate and my office-mate Yavuz Öztürk for being my closest friend. Simply, thanks for everything...

I would never forget my 'brother' Altan Çakır, from the precious undergraduate days. I'm expecting great collaboration between us in the near future. In your speech "My brother!"

I would never forget the help and motivation of Engin Durgun, Sefa Dağ, Deniz Çakir, Cem Sevik, Ayhan Yurtsever and my home-mates Nezih Türkçü, Cem Kuşçu, Faik Demirörs and Anıl Ağıral.

I would like to thank to all my friends in Physics Department for their friendship.

I am thankful to the all the members of "Atatürkçü Düşünce Derneği" both in İzmir and Ankara.

I would like to thank to Funda Güney for her moral support in my hard times and endless love... Thank you for everything!..

I bless to my mother Suzan Tongay, my father Ergün Tongay for their endless love and support. I would like to thank to my sister Nazan Gezek, Pervin Villasenor Ville, my brother Mehmet Ali Aydın, and Ahmet Gezek, Dilek Aydın, Selim Gezek, Altay Gezek, Mert Aydın. But someone that I never forget their names are: Erol Üçer and Aysel Üçer. Thanks for everything. Thanks for being my close relatives. Thanks for supporting me starting from my high school education to graduate study both financially and morally. I'm really very happy to be one of the member of my family. And all of my success in past, previous and future is not mine but all of these people that I have mentioned and cannot mentioned...

Contents

List of Figures

List of Tables

Chapter 1

Introduction

Importance of nanotechnology was first pointed out by Richard Feynman as early as in 1959. In his now famous lecture entitled , "There is Plenty of Room at the Bottom.", he stimulated his audience with the vision of exciting future discoveries if one could fabricate materials and devices at the atomic/molecular scale. He pointed out that, for this to happen, a new class of miniaturized instrumentation would be needed to manipulate and measure the properties of these small-"nano"-structures. But at that time, it was not possible for researchers to manipulate single atoms or molecules because they were far too small to be dedected by the existing tools. Thus, his speech was completely theoretical, but fantastic. He described how the laws of physics do not limit our ability to manipulate single atoms and molecules. Instead, it was our lack of the appropriate methods for doing so. However, he correctly predicted that the time would come in which atomically precise manipulation of matter would inevitably arrive.

It was not until the 1980s that instruments were invented with the capabilities Feynman envisioned. These instruments, including scanning tunnelling microscopes, atomic force microscopes, and near-field microscopes, provide the "eyes" and "fingers" required for nanoscale measurements and atomic manipulations. In a parallel development, expansion of computational capability now enables sophisticated simulations of material behavior at the nanoscale. These new tools and techniques have sparked excitement throughout the scientific community.

Traditional models and theories for material properties and device operations involve assumptions based on "critical length scales" which are generally larger than several nanometers. When at least one dimension of a material structure is under the critical length, distinct behavior often emerges that cannot be explained by traditional or classical models and theories. Thus, scientists from many disciplines are avidly fabricating and analyzing nanostructures for the advancement of nanoscience and nanotechnology.

Nowadays science society defines nanotechnology as the ability to work at the molecular level, atom by atom, to create large structures with fundamentally new molecular organization. Compared to the behavior of bulk materials, nanostructures in the range of about 10^{-9} to 10^{-7} m (1 to 100 nm - a typical dimension of 10 nm is 1,000 times smaller than the diameter of a human hair) exhibit important changes. Nanotechnology is concerned with materials and systems whose structures and components exhibit novel and significantly improved physical, chemical, and biological properties, phenomena, and processes due to their nanoscale size. The aim is to exploit these properties by gaining control of structures and devices at atomic, molecular, and supramolecular scale and to learn how to efficiently manufacture these devices. Maintaining the stability of interfaces and the integration of these "nanostructures" at the micron-length scale and macroscopic scale is another objective

New behavior at the nanoscale is not necessarily predictable from that observed at large size scales. The most important changes in behavior are caused not by the order of magnitude size reduction, but by newly observed phenomena intrinsic to or becoming predominant at the nanoscale, such as size confinement, predominance of interfacial phenomena and quantum mechanics. Once it is possible to control feature size, it is also possible to enhance material properties and device functions beyond those that we currently know or even consider as feasible. Reducing the dimensions of structures leads to entities, such as carbon nanotubes, nanowires and quantum dots, DNA-based structures, and laser emitters, which have unique properties. Such new forms of materials and devices herald a revolutionary age for science and technology, provided we can discover and fully utilize the underlying principles.

Materials and Manufacturing. Nanotechnology is fundamentally changing the way materials and devices will be produced in the future. The ability to synthesize nanoscale building blocks with precisely controlled size and composition and then to assemble them into larger structures with unique properties and functions will revolutionize segments of the materials manufacturing industry. At present we perceive only the tip of the iceberg in terms of the benefits that nano structuring can bring: lighter, stronger, and programmable materials; reductions in life-cycle costs through lower failure rates; innovative devices based on new principles and architectures; and use of molecular/cluster manufacturing, which takes advantage of assembly at the nanoscale level for a given purpose. We will be able to develop structures not previously observed in nature. Challenges include synthesis of materials by design, development of bio- and bio-inspired materials, development of cost-effective and scalable production techniques, and determination of the nanoscale initiators of materials failure.

Nanoelectronics and Computer Technology. Within ten years of the fundamental discovery of the new phenomenon of giant magnetoresistance, this nanotechnology completely replaced older technologies for computer disk heads and opened new market worth $34 billion in 1998. Other potential breakthroughs include (a) nanostructured microprocessor devices which continue the trend in lower energy use and cost per gate, thereby improving the efficacy of computers by a factor of millions; (b) communications systems with higher transmission frequencies and more efficient utilization of the optical spectrum to provide at least ten times more bandwidth, with consequences in business, education, entertainment, and defense; (c) small mass storage devices with capacities at multi-terabit levels, one thousand times better than today; and (d) integrated nanosensor systems capable of collecting, processing, and communicating massive amounts of data with minimal size, weight, and power consumption. Potential applications of nanoelectronics also include affordable virtual reality stations that provide individualized teaching aids (and entertainment); computational capability sufficient to enable unmanned combat and civilian vehicles; and communication capability that obviates much commuting and other business travel in an era of increasingly expensive transport fuels.

In the last decade, there has been a great interest in both geometrical, mechanical, electrical properties of nanowires and their fabrication. Nanowires are most important structures of nanoscience and nanotechnology since they have great potential in applied fields such as nanoelectronics as well as their very interesting nature. It's well known that the electrical and mechanical properties of any metal are not so different, whether its size is in millimeters or in meters. But, as soon as its size approaches the atomic size all common knowledge about the fundamental properties of these metals becomes invalid. For example, in Ohm's law, the electrical resistance of any metal is proportional to its length. However, since the distance an electron travels between two scattering events is typically much larger than the atomic size, this fundamental law breaks down. The electrons transverse the atomic sized conductor ballistically, and resistance becomes independent of its length. In fact, the character of the resistance changes conceptually and it will be necessary to invoke the wave nature of the electrons in the conductor for a proper description. The energy scales involved are much larger than that of the quantum effects become visible at room temperature. The chemical nature of the metals starts to play an essential role while the size gets smaller. As a result, while in macroscopic world any metal, say gold, with respect to the other metal,say lead, is better conductor, in nanoscaled dimensions this time lead is better than that of gold. Metal nanowires also exhibits very interesting quantum behavior, such as quantum of conductance, even at room temperature due to large energy level separation of the transport channels unlike in semiconductors. In addition to unusual electronic properties the mechanical properties by themselves are also quite unusual: plastic deformation in a macroscopic metal occur via structural dislocation motion. On the other hand, atomic sized metal wires flows in response to applied stresses via structural rearrangements and their yield strength is one or two orders of magnitude larger than for bulk materials.

The experimental investigation of these phenomena requires tools for manipulation and characterization of structure at the atomic and molecular scale. An important tools that make the fabrication of such nanowires possible are Scanning Tunnelling Microscope (STM) (which was developed by Gerd Binnig and

Heinrich Rohrer, for which they were awarded the nobel price in 1986) and High Resolution Electron Microscope (HRTEM) and Mechanical Controllable Break Junction (MCJB). One of the most important milestones in nanoscience is the fabrication of the stable gold monatomic chains suspended between two electrodes. Ohnishi et al [1], visualized these single atomic chains the first time by transmission electron microscopy (TEM). Concomitantly Yanson et al. [2] has produced four or five gold monatomic chain by using STM and MCJB, provided indirect evidence for their existence.

After having pioneered the idea of molecular electronics, where individual molecules plays the role of simple electronic device such as diod, transistor, tunnelling device, it is pointed out that the real challenge is in connecting these devices. In fact, the interconnects between molecular devices have crucial device elements as the device sizes have reduced at few nanometers.

Nanoelectronics has imposed the fabrication of stable and reproducible interconnects with the high conductivity with diameters smaller than that of the device that they are connected to. Nanowires have been produced first to investigate the coherent electron transport as fallow up of Gimzewski and Möller's experiment. Very thin metal wires and atomic chains have been produced by refracting the STM tip from an indentation and then by thinning the neck of materials that wets the tip. While these nanowires produced so far have played crucial role in understanding the quantum effects in electronic and thermal conductance they were neither stable nor reproducible to offer any relevant application. Recent research has shown that armchair nanotubes and nanowires, or metal coated carbon nanotubes can be served for this purpose and hence they make high conducting, nanometersize wires to connect these devices. Apart from being used as interconnects, nanowires have important aspects which attract the interest of researches.

If the atoms forming a wire have net magnetic moment, and also the wire itself have magnetic ground state, such a nanowire may offer applications as nanomagnets. This is expected to be an emerging field for data storage and electromagnetic devices.

In metallic electron densities, when the diameter of a wire becomes in the range of Broglie wave lenght (ie. $D \sim \lambda_B$) the energy level spacing of electronic and phononic states transversely confined to these wires become significant. Owing to that large level spacing, the quantized nature of electrons and phonons continue to be observable even at room temperature. As a result the electrical conductance **G** and heat conductance **K** exhibit quantized nature. The variation of **G** itself is clearly related with the atomic structure of the wire.

The structure of nanowires itself is important. The stability and periodicity of the atomic structure in one dimension (1D) is of academical and technological interest, because of our limited knowledge in crystallography in one dimension. Besides, earlier research have argued that at $D \sim \lambda_B$, the conductance G (even the diameter D or size) of nanowires are quantized. In this respect, we remind the reader from magic numbers of Si atom making silicon nanoclusters. Group IV elements, Carbon and Silicon, make semiconductor or insulator in diamond structure, because of their even number of valence electrons appropriate for tetrahedrally directed covalent bonds. Our interest in this thesis is to find their electronic properties when they form very thin nanowires.

In this thesis, we have studied the physical properties of carbon and silicon nanowires in detail. These two elements give many different stable nanowire structures which can be used as an interconnect between the nanodevices. In this thesis, various nanowires starting from carbon and silicon linear chain structure to more complex wires and their physical properties have been extensively discussed in chapter 4. Since tubes are another class of structure for one-dimensional nanowires, we focussed on the tubular structures of silicon. In the past decade several novel properties of carbon nanotubes have been investigated actively. These properties have been used to make prototypes of various electronic devices at nanoscale. In this thesis, we will not involve with the physical properties of carbon nanotubes. On the other hand, Si being in the same IV column as C atom, has similar structure and it is of intent to know whether Si has stable tubular structure. This way, additional tubular structures such as silicon (8,0) and (3,3) nanotubes also studied in detail. Calculated energy-band structure and density of states of these tubular structures attribute metallic properties to them. Although

Generalized Gradient Approximation (GGA) method gives stable structure, we applied stability test to the structure. Stability test can be applied in various ways as discussed in Chapter 4.3.1. In our work, we chose to deform the structures and then look for the relaxed positions of the atoms. In the second part, conduction of C1 and Si1 is calculated by Empirical Tight-Binding Method (ETBM). This method is discussed in Chapter 3 and Chapter 4.3.1.

This thesis is organized as follows: Chapter 2 gives a brief information about the physical properties of different types of nanowires. Chapter 3 summarizes the theoretical background, method of calculation and approximation methods, Chapter 4, presents results and discussion. This work ends by giving concluding remarks and suggestion for possible future work.

Chapter 2

Nanowires

2.1 Different types of nanowires

In the previous chapter we present an introductory explanation on the importance and fabrication of nanowires. In this chapter we will discuss different types of nanowires and their physical properties.

2.1.1 Single Nanowires

Nanowires have been produced by retracting the STM tip from nano indentation. The atoms of the sample, which wet the tip have formed a neck between the tip and sample. Metal wires having lengths as long as $\sim 400A^0$ were produced. However, the prime drawback in those wires produced by STM were irregularities in their structure. Since their size and structure were not controllable and not reproducible, serious technological applications involving those wires are not possible.

Earlier studies based on classical molecular dynamics calculations have shown that single atom nanowires can form. This finding confirmed experimentally by Ohnishi et al [1] and Yanson et al [2], who fabricated stable single atom chain

of Au between two electrodes. Later, first principle calculations demonstrated the stability and electronic structure of single atom chains by performing phonon calculation. Gulseren et al. [3] performed an extensive study using an empirical potential and determined the exotic structure of very thin nanowires of Al and Pb. However, lattice parameters Au deduced from experiment have been matter of dispute among various theoretical studies.

2.1.2 Single Wall Carbon Nanotubes (SWNTs)

After the synthesis of single wall carbon nanotubes (SWNTs) in 1993 by Bethune et al [5] and by Iijima et al. [4, 6], the focus of carbon research has shifted towards the SWNTs, especially through the development of an ancient synthesis method for their large scale production by Smalley and colleagues [7].

Nanotubes are simply rolled up structure of 2-D graphite layer which is specified as graphene layer.

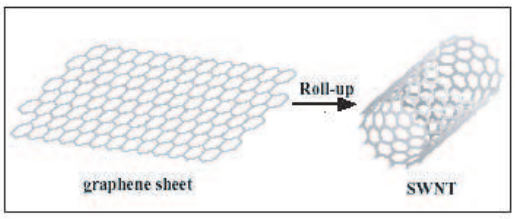

Figure 2.1: Representation single wall carbon nanotubes by rolling up the graphene layer.

Graphite is simply a 3 dimensional hexagonal lattice of carbon atoms, and each single layer of graphite structure is called graphene. In a graphene layer, sp_2 orbitals of nearest neighbort carbon atoms overlap with each other in order to make strong covalent bonds. The bonding combination of two sp^2 orbitals gives the most stable bonding, which is called σ bonding.

The physical properties of SWNTs depend on the diameter and chirality, which are defined by the indices (n,m). Chirality is a term used to specify a

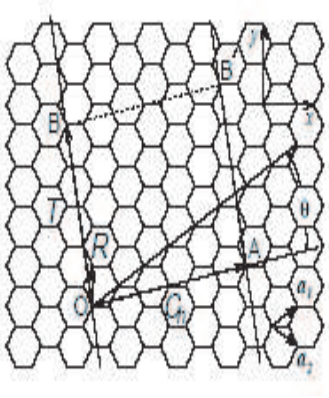

Figure 2.2: Carbon nanotube is a single layer of graphite rolled into a cylinder.

nanotube structure, which does not have mirror symmetry. The structure of a SWNTs is specified by the vector C_h, and this vector is written as follows,

$$\mathbf{C_h} = n\mathbf{a_1} + n\mathbf{a_2} \tag{2.1}$$

where $\mathbf{a_1}$ and $\mathbf{a}_2$ are unit vectors of the hexagonal lattice shown in Fig. 2.2 . The vector $\mathbf{C}_h$ connects two crystallographically equivalent sites O and A on a two-dimensional graphene sheet, where a carbon atom is located at each vertex of the honeycomb structure. When we join the line AB' to the parallel line OB in Fig. 2.2, we get a seamlessly joined SWNT which is classified by the integers (n,m), since the parallel lines AB' and OB cross the honeycomb lattice at equivalent points. There are only two kinds of SWNTs, which have mirror symmetry: zigzag nanotubes (n,0), and armchair nanotubes (n,n). The other nanotubes are called chiral nanotubes. A chiral nanotube has C-C bonds that are not parallel to the nanotube axis, denoted by the chiral angle θ. Here the direction of the nanotube axis corresponds to OB. The zigzag, armchair and chiral nanotubes correspond, respectively, to Θ=0^0, Θ=30^0 and $0 \leq \Theta \leq 30^0$. In a zigzag (armchair) nanotube one of three C-C bonds from a carbon atom is parallel (perpendicular) to the nanotube axis.

Since the quantum properties of the single wall carbon nanotube depend on

the diameter and chirality, it will be suitable to indicate the diameter of a (n,m) nanotube d_t,

$$d_t = C_h/\pi = \sqrt{3}a_{c-c}(m^2 + mn + n^2)^{1/2}/\pi \tag{2.2}$$

where a_{c-c} is the nearest-neighbour C-C distance (1.42 Angstrom in graphite), and C_h is the lenght of the chiral vector C_h. The chiral angle θ can be given by,

$$\theta = \tan^{-1}[\sqrt{3}m/(m + 2n)]] \tag{2.3}$$

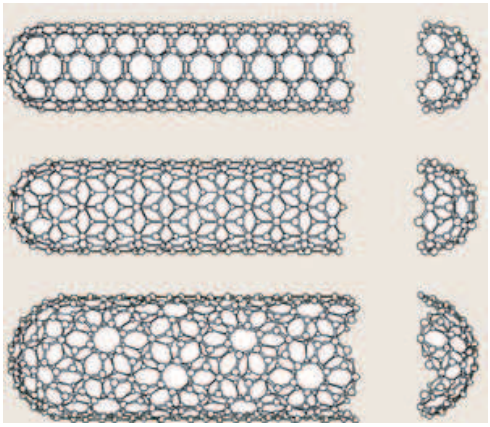

Figure 2.3: A (5,5) armchair nanotube (top), a (9,0) zigzag nanotube (middle) and a (10,5) chiral nanotube.

The electronic structure of SWNTs can be summarized as follows: In general, (n,m) tubes with n-m=3q ($n - m \neq 3q$), where q is an integer are metallic (semiconductor) [8]. Hence armchair nanotubes with (n,n) are metallic while zigzag nanotubes with (n,0) are metallic or semiconductor depending on whether n=3q or not. This behavior of nanotubes can be explained by zone-folding and the curvature effects [8].

2.1.3 Functionalized SWNTs

Physical properties of SWNTs can be modified by the adsorption of a foreign atom or molecule on the surface of the tube. Adsorption can take plane externally or internally. For example the band gap of a zigzag tube can be reduced by coverage of O_2. Exohydrogenation, i.e hydrogen atom coverage of a zigzag tube leads to the widening of the band gap. Transition metal adsorption give rise to permanent magnetic moment. The modification of physical properties through adsorption of atoms or molecules is called functionalization of SWNT [9].

2.1.4 Coated Carbon Nanotubes

Coating of SWNTs (i.e, molecular or multilayer atom adsorption on SWNTs) is of particular interest in the context of nanowires or conductors. It has been shown experimentally that semiconducting SWNTs can be coated quite uniformly by Ti atoms.First principle calculations by Dağ et al [10]. have shown that (8,0) tube can be uniformly covered by Ti atoms, and becomes a good conductor. Those studies clearly showed that metal atom coating of SWNTs can be used to formate interconnects with reproducible properties. Not all the atom can form uniform coverage, they rather appear as small particles on the surface of the SWNT. For example, good conductors such as Au, Ag and Cu cannot make uniform coating. This difficulty can be overcome by the coating of Au and Ag on the buffer layer of Ti or Ni, that can make uniform coverage of the surface of the tube.

SWNT coated by transition metal atoms are used not only for conductors, but for nanomagnets. The first principle calculations reveals that net magnetic moment can be created upon the coating of SWNT by atom such as Ti, Co, Cr etc.

2.2 Physical Properties of Nanowires

2.2.1 Electronic Structure

A finite nanowire between two metal electrodes displays discrete energy spectrum. The energy level spacing decreases as the number of atoms in the wire increases. As the lenght of nanowire increases these energy levels can be described by a band having dispersion along the axis of the wire. Under these circumstances, the wave vector along the axis starts to be a good quantum number. If the wire consists of a few atoms, the energy states give rise to resonances.

2.2.2 Quantum Conductance

The discrete nature of electronic and phononic states of nanowire connecting two electrodes reflects to the electrical and thermal conductance between two electrodes connected by this wire. At the end it yields resorvable effects in measured conductance.

The conductance of large samples obeys Ohm's law, namely, G=σS/L, where S is the cross section and L is the lenght. At microscopic scale, which are measured in nanometer, the behavior of conductance, namely its variation with the L or S differs from that in macroscopic scale. Firstly there is an interface resistance independent of the lenght L of the sample. Secondly the conductance does not decrease uniformly with the width W. Instead it depends on the number of transverse modes in the conductor and goes down in discrete steps (of quantum conductance $2e^2$/h). The Landauer formula incorporates both of these features [37].

$$G = \frac{2e^2}{h} \sum n_i T_i \tag{2.4}$$

Here n_i is the degeneracy of the propagating modes, and the factor T transmission coefficient, i.e. represents the average probability that an electron injected at one end of the conductor will transmit to the other end through the channel i. If the transmission probability is unity, then we recover the correct expression for the resistance of a ballistic conductor.

After introducing Landauer formula, now we can discuss the conductance of nanotubes and nanowires. The conductance of the (n,n) armchair SWNTs can be estimated from the number of bands crossing E_F. There are two p_x derived bands at the Fermi level, one even and one odd parity under the n axial mirror symmetries of the tube. Therefore one expects that a single armchair nanotube has a conductance of $(T_e+T_o)G_0$, where T_e and T_o are the transmission coefficients associated with parity. If the transmission coefficients are unity, we then get a conductance of $2G_0$ where $G_0 = 2e^2/h$ at the Fermi level. If we generalize this for MWNTs which is composed of m individual tubes, each having two channels at the Fermi level, the maximum ballistic conductance is thus $2mG_0$ However, experiments showed $G = G_0$ rather than $G = 2G_0$

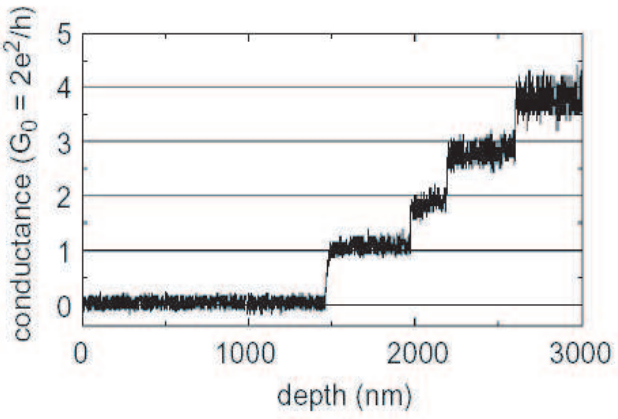

Figure 2.4: Conductance G at room temperature measured as a function of depth of immersion of the nanotube bundle into the liquid gallium. As the nanotube bundle is dipped into the liquid metal, the conductance increases in steps of G_0=$2e^2$/h. The steps corresponds to different nanotubes coming successively into the contact with the liquid. [11]

But this puzzling situation has been clarified by Ihm and Louie [12] The

incident π^* band electrons have a very high angular momentum with respect to the tube axis, and these electrons go through the tube without being scattered by the free electrons in surrounding metal and contribute a quantum unit ($2e^2$/h) to the conductance. On the other hand, the incident π band electrons, with the p_z atomic orbitals in phase along the tube circumference, experience strong resonant back-scattering because the low-angular-momentum states at the Fermi level have a dominantly metallic character in the nanotube jellium metal coexistence region. So these results obtained by Ihm and Louie provide an explanation for the experimentally observed conductance of one quantum unit instead of two for nanotubes with one end dipped into liquid metal such as gallium. Fig. 2.4

Having discussed the quantum conductance of nanotubes, further discussion about the quantum conductance of nanowires is in order. On the basis of ab initio calculations it has been shown that the conductance depends on the valence states as well as the site where the single atom is bound to the electrode [13]. The coupling to electrodes and hence the transmission coefficients are expected to depend on the binding structure. Scheer et al [14] found a direct link between valence orbitals and the number of conduction channels in the conductance through a single atom. Lang [15] calculated the conductance through a single Na atom, as well as a monatomic chain comprising two, three and four Na atoms between two jellium electrodes by using the Green's function formalism. He found an anomalous dependence of the conductance on the lenght of the wire. The conductance through a single atom was low (about $G_0/3$), but increased by a factor of two in going from a single atom to the two-atom wire. This behavior was explained as the incomplete valence resonance of a single Na atom interacting with the continuum of states of the jellium electrodes. Each additional Na atom modifies the electronic structure and shifts the energy levels. The closer a state is to the Fermi level, the higher is its contribution to the electrical conductance. According to the Kalmeyer-Laughlin theory [16], a resonance with the maximum DOS at the Fermi level makes the highest contribution to the transmission; the conductance decreases as the maximum shifts away from the Fermi level.

This explanation is valid for a single atom between two macroscopic electrodes forming a neck with length $l < \lambda_F$. The situation is, however, different for long

monatomic chains. Since the electronic energy structure of a short monatomic chain varies with the number of atoms, the results are expected to change if one goes beyond the jellium approximation and considers the details of the coupling of chain atoms to the electrode atoms. It is also expected that the conductance will depend on where the monatomic chain ends and where the jellium edge begins. In fact, Yanson et al [17] argued that the conductance of the Na wire calculated by Lang [18] is lower than the experimental value possibly due to the interface taken with the jellium.

2.2.3 Thermal Conductance

In nanowires thermal transport occurs by phonons and electrons. In dielectric wires the energy is transported only by phonons, but in metalic wires this transportation occurs mainly by electrons, since phononic contribution is small. Therefore, in discussing the thermal transportation through wires, it will be suitable to distinguish the thermal conductance through electrons and phonons.

When the width of the constriction of lenght l and width w is in the range of Fermi wavelength, the transverse motion of electrons confined to w becomes quantized. The finite level spacing of the quantized electronic states reverberates into the ballistic electron transport, and gives rise to resolvable quantum features in the variation of electrical and thermal conductance.

The phononic thermal conductance through a perfect and infinite chain, K_p, is calculated by Buldum, Ciraci and Fong [19] by using a model Hamiltonian approach, has been expressed as

$$K_p = \sum(\pi^2 k_b^2/3h)T \tag{2.5}$$

Accordingly the ballistic thermal conductance of each branch i of the uniform and harmonic atomic chain is limited by the value $K_0 = \pi^2 k_b^2 T/3h$. It is independent of any material parameter, and is linearly dependent on $T = (T_L + T_R)/2$.

The total thermal conductance becomes $K_p = NK_0$, where N is the total number of phonon branches. For an ideal 1D atomic chain, N=3, if the transverse vibrations are allowed. Furthermore, Ozpineci and Ciraci [20], showed that the phononic thermal conductance through dielectric atomic chain having 1-10 atoms exhibits features similar to that found in the ballistic electrical conductance through similar atomic chains.

Chapter 3

Theoretical Background

3.1 Born-Oppenheimer Approximation

Since the electrons have small mass compared with mass of the nuclei, electrons move much faster than nuclei. So this means that electrons have the ability to follow the motion of the nuclei instantaneously, so they remain in the same stationary state of the electronic Hamiltonian all the time [21].This stationary state will vary in time because of the coulombic coupling of these two sets of freedom. So this means that as the nuclei follow their dynamics, the free electrons instantaneously adjust their wavefunction according to the nuclear wavefunction. Within these conditions, full wavefunction can be expressed as follows;

$$\Psi(\mathbf{R},\mathbf{r},\mathbf{t}) = \Theta(\mathbf{R},t)\Phi(\mathbf{R},\mathbf{r}) \tag{3.1}$$

Here nuclear wave function $\Theta(\mathbf{R},t)$ obeys the time-dependent Schrödinger equation and electronic wave function $\Phi(\mathbf{R},\mathbf{r})$ is the m-th stationary state of the electronic Hamiltonian where m is any electronic eigenstate, but most of the applications in the literature are focused on the ground state, i.e m=0.

Since the nuclear wavefunction satisfies the time-dependent Schrödinger equation, we can easily construct the time-dependent Schrödinger equation. But solving this equation is a formidable task for mainly two reasons; first of all it is a many-body equation in N (N:number of atoms) nuclear coordinates, where the interaction potential being given in a implicit form. Secondly the determination of the potential energy surface for every possible nuclear configuration $\mathbf{R}$ involves M^N times the electronic equation, where M is defined as typical number of grid points. However in many cases of our interest this nuclear solution is not necessary since the thermal wavelength for a particle of mass M is $\lambda_T = (\frac{e^2}{Mk_bT})$, so the regions of space separated by more than λ_L do not exhibit quantum coherence and potential energy surfaces in typical bonding environments are stiff enough to localize the nuclear wavefunctions to large extent.

Assuming these approximations, now we are left with the problem of solving the many-body electronic Schrödinger equation for fixed nuclear positions.

3.2 The Electronic Problem

Although we are left with only solving the electronic part, solving Schrödinger equation for a system of N interacting particle electrons in an external field is still very difficult problem in many-body theory. The numerical solution is known only in the case of uniform electron gas (for atoms with small number of electrons and for a few molecules). For getting the analytical solution we have to resort to approximations.

To cope with many electron Hamiltonian in 1928 Hartree proposed that many-electron wave function (electronic wavefunction) can be written as product one-electron wave functions each of which satisfies one-particle Schrödinger equation in an effective potential. [22]

$$\Phi(\mathbf{R}, \mathbf{r}) = \Pi_i \varphi(\mathbf{r}_i) \tag{3.2}$$

$$(-\frac{\hbar^2}{2m}\nabla^2 + V_{eff}^{(i)}(\mathbf{R},\mathbf{r}))\varphi_i(\mathbf{r}) = \epsilon_i\varphi_i(\mathbf{r}) \tag{3.3}$$

with effective potential

$$V_{eff}^{(i)}(\mathbf{R},\mathbf{r}) = V(\mathbf{R},\mathbf{r}) + \int \frac{\sum_{j\neq i}^{N}\rho_j(\mathbf{r'})}{|\mathbf{r}-\mathbf{r'}|}d\mathbf{r'} \tag{3.4}$$

where

$$\rho_j(\mathbf{r}) = |\phi_j(\mathbf{r})|^2 \tag{3.5}$$

is the electronic density associated with particle j. The second term in Eq. 3.4 is the mean field potential and the third term is the interactions of one electron with the other electrons in a mean field. But it should be noted that total energy of the many-body system is not just the sum of the eigenvalues of Eq. 3.3 because the formulation in terms of an effective potential makes the electron-electron interaction to be counted twice. So that the correct expression for the energy is written as

$$E^H = \sum_i^N \varepsilon_n - \frac{1}{2}\int\int \frac{\rho(\mathbf{r})\rho(\mathbf{r'})}{|\mathbf{r}-\mathbf{r'}|}d\mathbf{r}d\mathbf{r'} \tag{3.6}$$

where second term is correction due to effective potential as discussed above. Wavefunctions $\Phi_i(\widehat{r})$ and charge density $\rho(r)$, as well as ϵ_i energies are determined by using self-consistent field (SCF) method.

Hartree approximation can be improved by considering the fermionic nature of electrons. Due to Pauli exclusion principle, two fermions (electrons in our case) cannot occupy the same state with all of their quantum numbers are the same. In this case electronic wavefunction in 3.2 becomes an antisymmetrized many-body electron wavefunction in the form of a Slater determinant as follows;

$$\Phi(\mathbf{R},\mathbf{r}) = \frac{1}{\sqrt{N!}}\begin{pmatrix} \phi_1(\mathbf{r_1}) & \dots & \phi_1(\mathbf{r_N}) \\ \vdots & \ddots & \vdots \\ \phi_N(\mathbf{r_1}) & \dots & \phi_N(\mathbf{r_N}) \end{pmatrix} \tag{3.7}$$

This approximation is called Hartree-Fock (HF) and it explains particle exchange in an exact manner [23, 24]. It also provides a moderate description of

inter-atomic bonding but many-body correlations are completely absent. Recently, the HF approximation is routinely used as a starting point for more advanced calculations. It should be also noted that although HF equations look same as Hartree equations, there is an additional coupling term in the differential equations.

Parallel to the development in electronic theory, Thomas and Fermi proposed, at about same time as Hartree, that the full electron density was the fundamental variable of the many-body problem, and derived a differential equation for the density without referring to one-electron orbitals. Although, this theory which known as Thomas-Fermi Theory [25, 26], did not include exchange and correlation effects and was able to sustain bound states, it set up the basis of later development of Density Functional Theory (DFT).

3.3 Density Functional Theory

The initial work on DFT was reported in two publications: first by Hohenberg-Kohn in 1964 [27], and the next by Kohn-Sham in 1965 [28]. This was almost 40 years after Schrödinger (1926) had published his pioneering paper marking the beginning of wave mechanics. Now Density Functional Theory is very powerful method for solving N interacting electron system.

The total ground state energy of an inhomogeneous system composed by N interacting electrons includes three terms, namely kinetic energy $\widehat{T}$, interaction with external fields $\widehat{V}$ and electron-electron interaction $\widehat{U_{ee}}$;

$$E = \langle \widehat{T} \rangle + \langle \widehat{V} \rangle + \langle \widehat{U_{ee}} \rangle \tag{3.8}$$

Before concentrating on the electron-electron interaction term, we can indicate the kinetic energy and interaction with external fields terms as follows;

$$V = \sum_{I=1}^{P} \langle \Phi | \sum_{i=1}^{N} \upsilon(r_i - R_I) | \Phi \rangle = \sum_{I=1}^{P} \int \rho(r) \upsilon(r - R_I) dr \tag{3.9}$$

$$T = \langle \Phi | \frac{-\hbar^2}{2m} \sum_{i=1}^{N} \nabla_i^2 | \Phi \rangle = -\frac{\hbar^2}{2m} \int [\nabla_r^2 \rho_1(r, r')]_{r'=r} dr \tag{3.10}$$

Returning back to electron-electron interaction term, this can be written by considering the coulomb interaction between them,

$$\widehat{U_{ee}} = \langle \Phi | \widehat{U_{ee}} | \Phi \rangle = \langle \Phi | \frac{1}{2} \sum_{i=1}^{N} \sum_{j \neq i}^{N} \frac{1}{\mid (r_i - r_j) \mid} | \Phi \rangle = \int \frac{\rho_2(r, r')}{\mid (r - r') \mid} dr dr' \tag{3.11}$$

By redefining $\rho_2(r, r')$ by using the two-body direct correlation function $g(r, r')$ and the one-body density matrix $\rho(r, r')$ as in Eq. 3.12, Eq. 3.11 simplify to Eq. 3.13

$$\rho_2(r, r') = \frac{1}{2} \rho(r, r) \rho(r, r') g(r, r') \tag{3.12}$$

$$U_{ee} = \frac{1}{2} \int \frac{\rho(r)\rho(r')}{\mid (r - r') \mid} dr dr' + \frac{1}{2} \int \frac{\rho(r)\rho(r')}{\mid (r - r') \mid} [g(r, r') - 1] dr dr' \tag{3.13}$$

It is obvious that the first term is the classical electrostatic interaction energy corresponding to a charge distribution $\rho(r)$ and the second term includes the classical and quantum correlation effects. By introducing *exchange depletion* written in Eq. 3.14 instead $g(r, r')$, we achieve another expression for total energy of many-body electronic system Eq. 3.15.

$$g_x(r, r') = 1 - \frac{\sum_\sigma \mid \rho_\sigma^{HF}(r, r') \mid^2}{\rho^{HF}(r) \rho^{HF}(r')} \tag{3.14}$$

$$E = T + V + \frac{1}{2} \int \frac{\rho(r)\rho(r')}{\mid (r - r') \mid} dr dr' + E_{xc} \tag{3.15}$$

In this equation the last term corresponds to exchange and correlation energy, and this can be expressed as follows,

$$E_{xc} = \frac{1}{2}\int \frac{\rho(r)\rho(r')}{\mid (r-r') \mid}[g(r,r')-1]drdr' \tag{3.16}$$

3.3.1 Hohenberg-Kohn Formulation

The Hohenberg-Kohn [27] formulation of DFT can be explained by two theorems:

Theorem 1: The external potential is univocally determined by the electronic density, except for a trivial additive constant.

Since $\rho(\mathbf{r})$ determines V($\mathbf{r}$), then this also determines the ground state wavefunction and gives the full Hamiltonian for the electronic system. So that $\rho(\mathbf{r})$ determines implicitly all properties derivable from H through the solution of the time-dependent Schrödinger equation.

Theorem 2: The minimal principle can be formulated in terms of trial charge densities, instead of trial wavefunctions.

The ground state energy E could be obtained by solving the Schrödinger equation directly or from the Rayleigh-Ritz minimal principle:

$$E = min\frac{\langle\widetilde{\Psi}|H|\widetilde{\Psi}\rangle}{\langle\widetilde{\Psi}|\widetilde{\Psi}\rangle} \tag{3.17}$$

Using $\widetilde{\rho}(\mathbf{r})$ instead of $\widetilde{\Psi}(\mathbf{r})$ was first presented in Hohenberg and Kohn. For a non-degenerate ground state, the minimum is attained when $\widetilde{\rho}(\mathbf{r})$ is the ground state density. And energy is given by the equation:

$$E_V[\widetilde{\rho}] = F[\widetilde{\rho}] + \int \widetilde{\rho}(\mathbf{r})V(\mathbf{r})d\mathbf{r} \tag{3.18}$$

with

$$F[\widetilde{\rho}] = \langle\Psi[\widetilde{\rho}]|\widehat{T}+\widehat{U}|\Psi[\widetilde{\rho}]\rangle \tag{3.19}$$

and $F[\widetilde{\rho}]$ requires no explicit knowledge of V($\mathbf{r}$).

These two theorems form the basis of the DFT. The main remaining error is due to inadequate representation of kinetic energy and it will be cured by representing Kohn-Sham equations.

3.3.2 Kohn-Sham Equations

Thomas and Fermi gave a prescription for constructing the total energy in terms only of electronic density by using the expression for kinetic, exchange and correlation energies of the homogeneous electron gas to construct the same quantities for the inhomogeneous system [28]. This was the first time that the *Local Density Approximation* (LDA) was used. But this model is a severe shortcoming since this does not hold bound states and also the electronic structure is absent!!!

W.Kohn and L.Sham then proposed that the kinetic energy of the interacting electrons can be replaced with that of an equivalent non-interacting system which can be calculated easily. With this idea, the density matrix $\rho(r, r')$ of an interacting system can be written as sum of the spin up and spin down density matrices,

$$\rho_s(r, r') = \sum_{i=1}^{\infty} n_{i,s} \Phi_{i,s}(r) \Phi_{i,s}^*(r') \tag{3.20}$$

Where $n_{i,s}$ ar the occupation numbers of single particle orbitals, namely $\Phi_{i,s}(r)$. Now the kinetic energy term can be written as Eq. 3.21

$$T = \sum_{s=1}^{2} \sum_{i=1}^{\infty} n_{i,s} \langle \Phi_{i,s} | -\frac{\nabla^2}{2} | \Phi_{i,s} \rangle \tag{3.21}$$

This expression can be developed by considering that the Hamiltonian has no electron-electron interactions and thus eigenstates can now be expressed in the form of Slater determinant. By using this argument the density is written as

$$\rho(\mathbf{r}) = \sum_{s=1}^{2}\sum_{i=1}^{N_s} |\varphi_{i,s}(\mathbf{r})|^2 \tag{3.22}$$

and the kinetic term becomes

$$T[\rho] = \sum_{s=1}^{2}\sum_{i=1}^{N_s} \langle\varphi_{i,s}| -\frac{\nabla^2}{2}|\varphi_{i,s}\rangle \tag{3.23}$$

Now, we can write the total energy of the system which is indicated in Eq. 3.15 in terms only of electronic density as follows,

$$E_{Kohn-Sham}[\rho] = T[\rho] + \int \rho(\mathbf{r})v(\mathbf{r})d\mathbf{r} + \frac{1}{2}\int\int \frac{\rho(\mathbf{r})\rho(\mathbf{r}')}{|\mathbf{r}-\mathbf{r}'|}d\mathbf{r}d\mathbf{r}' + E_{XC}[\rho] \tag{3.24}$$

This equation is called the *Kohn-Sham Equations* After writing main equation, now the solution of the Kohn-Sham equations can be achieved by applying the same iterative procedure, in the same way of Hartree and Hartree-Fock equations. As a remark after all, in this approximation we have expressed the density functional in terms of KS orbitals which minimize the kinetic energy under the fixed density constraint. In principle these orbitals are a mathematical object constructed in order to render the problem more tractable, and do not have a sense by themselves.

3.4 Exchange and Correlation

If we know the exact expression for the kinetic energy including correlation effects, then we can use the original definition of the exchange-correlation energy $E^0_{XC}[\rho]$ which does not contain kinetic contributions.

$$E^0_{XC}[\rho] = \frac{1}{2}\int\int \frac{\rho(r)\rho(r')}{|\ (r-r')\ |}[g(r,r')-1]drdr' \tag{3.25}$$

In this equation $E^0_{XC}[\rho]$ is the exchange-correlation energy without kinetic contributions. For writing the exchange-correlation energy $E_{XC}[\rho]$ as a function of ρ, we redefine Eq. 3.25 by considering the non-interacting expression for the kinetic energy $T_R[\rho]$ in the following way,

$$E_{XC}[\rho] = E^0_{XC}[\rho] + T[\rho] - T_R[\rho] \tag{3.26}$$

In this equation second term is interacting kinetic energy with correlation effects, while the last term corresponds to non-interacting kinetic energy. These two term can be considered as a modification to two-body correlation function $g(r, r')$ in Eq. 3.25. Updated two-body correlation function is now called as *average of pair correlation function*, and the exchange-correlation energy with kinetic contribution can be written as,

$$E_{XC}[\rho] = \frac{1}{2}\int\int \frac{\rho(r)\rho(r')}{\mid (r-r') \mid}[\widetilde{g}(r, r') - 1]drdr' \tag{3.27}$$

where $\widetilde{g}(r, r')$ can be expressed as follows,

$$\widetilde{g}(r, r') = 1 - \frac{\sum_\sigma \mid (\rho_\sigma(r, r') \mid^2)}{\rho(r)\rho(r')} + \widetilde{g_{xc}(r, r')} \tag{3.28}$$

For further simplification for $E_{XC}[\rho]$, the exchange-correlation hole $\widetilde{g_{xc}(r, r')}$ is defined

$$\widetilde{g_{xc}(r, r')} = \rho(r')[\widetilde{g}(r, r') - 1] \tag{3.29}$$

so $E_{XC}[\rho]$ becomes,

$$E_{XC}[\rho] = \frac{1}{2}\int\int \frac{\rho(r)\widetilde{g_{xc}(r, r')}}{\mid (r-r') \mid}drdr' \tag{3.30}$$

Having discussed fundamental equations of DFT, we introduce next the *Local Density Approximation* (LDA) and *Generalized Gradient Approximation* (GGA)

3.4.1 Local Density Approximation (LDA)

The local density approximation has been the most widely used approximation to handle exchange correlation energy. It has been proposed in the seminal paper by Kohn and Sham, but the philosophy was already present in Thomas-Fermi theory. In Local Density Approximation, the exchange-correlation energy of an electronic system is constructed by assuming that the exchange-correlation energy per electron at a point ρ in the electron gas, is equal to the exchange-correlation energy per electron in a homogeneous electron gas that has the same electron density at the point ρ. In fact LDA based on two main approximations, (1) The pair function is approximated by that of the homogeneous electron gas density $\rho(r)$ corrected by the density ratio $\rho(r)/\rho(r')$ to compansate the fact that the LDA exchange-correlation hole is now centered at r instead of r' (2) The LDA exchange-correlation hole interacts with the electronic density at r, and is centered at r. But as we know that the real exchange-correlation hole is actually centered at r' instead r.

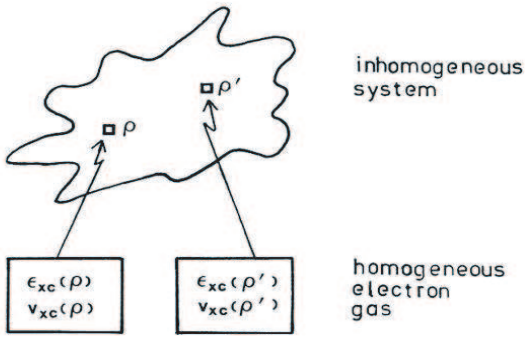

Figure 3.1: Schematic representation of Local Density Approximation

3.4.2 Generalized Gradient Approximation (GGA)

Although the LDA was the universal choice for ab-initio calculations on amorphous systems, there were well known problems with the approximation: (1) First of all in the local density approximation the optical gap is always poorly estimated (normally underestimated). Of course, this does not affect ground state properties like charge density, total energy and forces, but it serious problem for calculations of conduction states, as for example in the case of transport or optical properties.(2) In strongly (electronically) inhomogeneous systems such as SiO, the basic assumption of weak spatial variation of the charge density is not well satisfied, hence the LDA has difficulty. (3) The LDA assumes that the system is paramagnetic; the local spin density approximation [34] (LSDA) (in which a separate "spin up" and "spin down" density functional is used) is useful for systems with unpaired spins, as for example a half filled state at the Fermi level.

Several workers, but especially Perdew [35], have worked on next step to the LDA: inclusion of effects proportional to the gradient of the charge density. Recent improvements along these ways are called *Generalized Gradient Approximations* (GGA), it seems that these have led to significant improvements in SiO [36], and intermolecular binding in water is better described with GGA than in the LDA. In some ways the GGA has been disappointing; on very precise measurements on molecules the results have been mixed. But overall, the GGA seems to be an improvement over the conventional LDA.

In GGA exchange-correlation energy can be written as follows,

$$E_{XC}[\rho] = \int \rho(\mathbf{r})\epsilon_{XC}[\rho(\mathbf{r})]d\mathbf{r} + \int F_{XC}[\rho(\mathbf{r}, \nabla\rho(\mathbf{r}))]d\mathbf{r} \tag{3.31}$$

where the function F_{XC} is asked to satisfy the formal conditions.

GGA approximation improves binding energies, atomic energies, bond lengths and bond angles when compared the ones obtained by LDA. In our calculations, we used the GGA approximation [45].

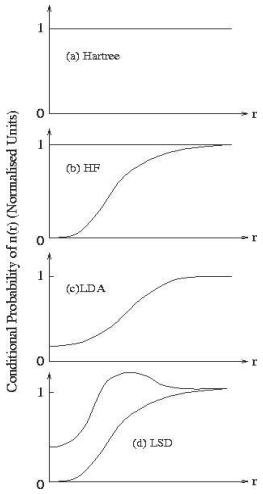

Figure 3.2: Summary of the electron-electron interactions where the coulombic interactions excluded. (a) the Hartree approximation, (b) the Hartree-Fock approximation, (c) the local density approximation and (d) the local spin density approximation which allows for different interactions for like-unlike spins.

As a summary of all approximations Fig. 3.2 will be useful for the reader.

3.5 Other Details of Calculations

By using the represented formalisms observables of many-body systems can be transformed into single particle equivalents. However, there still remains two difficulties: A wave function must be calculated for each of the electrons in the system and the basis set required to expand each wave function is infinite since they extend over the entire solid.

k-point Sampling : Electronic states are only allowed at a set of **k**-points determined by boundary conditions. The density of allowed **k**-points are proportional to the volume of the cell. The occupied states at each **k**-point contribute to the electronic potential in the bulk solid, so that in principle, an finite number of calculations are needed to compute this potential. However, the electronic wave functions at **k**-points that are very close to each other, will be almost identical.

Hence, a single **k**-point will be sufficient to represent the wave functions over a particular region of **k**-space. There are several methods which calculate the electronic states at special **k**-points in the Brillouin zone [47]. Using these methods one can obtain an accurate approximation for the electronic potential and total energy at a small number of **k**-points. The magnitude of any error can be reduced by using a denser set **k**-points.

Plane-wave Basis Sets : According to Bloch's theorem, the electronic wave functions at each **k**-point can be extended in terms of a discrete plane-wave basis set. Infinite number of plane-waves are needed to perform such expansion. However, the coefficients for the plane waves with small kinetic energy $(\hbar^2/2m)|\mathbf{k}+\mathbf{G}|^2$ are more important than those with large kinetic energy. Thus some particular cutoff energy can be determined to include finite number of **k**-points. The truncation of the plane-wave basis set at a finite cutoff energy will lead to an error in computed energy. However, by increasing the cutoff energy the magnitude of the error can be reduced.

Plane-wave Representation of Kohn-Sham Equations : When plane waves are used as a basis set, the Kohn-Sham(KS) [28] equations assume a particularly simple form. In this form, the kinetic energy is diagonal and potentials are described in terms of their Fourier transforms. Solution proceeds by diagonalization of the Hamiltonian matrix. The size of the matrix is determined by the choice of cutoff energy, and will be very large for systems that contain both valence and core electrons. This is a severe problem, but it can be overcome by considering pseudopotential approximation.

Nonperiodic Systems : Bloch theorem cannot be applied to a non-periodic systems, such as a system with a single defect. A continuous plane-wave basis set would be required to solve such systems. Calculations using plane-wave basis sets can only be performed on these systems if a periodic supercell is used. Periodic boundary conditions are applied to supercell so that the supercell is reproduced through out the space. As seen schematically in Fig. 3.3 even a molecule can be studied by using a supercell which prevents interactions between molecules.

Pseudopotential Approximation : Numerically and mathematically, a

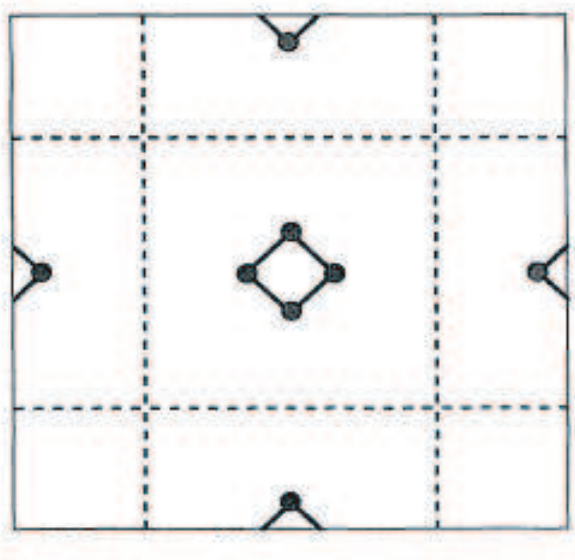

Figure 3.3: Supercell geometry for a molecule. Supercell is chosen large enough to prevent interactions between the nearest neighbor molecules.

plane wave basis is the most convenient basis set to be implemented for crystals. However, the plane wave basis set suffers from the slow convergence in the presence of core potential of atom's. Convergence drawback is circumvented by the use of pseudopotential approximation. The core electrons are relatively unaffected by the chemical environment of an atom. Hence it will be convenient to assume that their (large) contribution to the total binding energy does not change when isolated atoms are brought together to form a molecule or crystal. In fact the actual energy differences of interest are the changes in valence electron energies, and so if the binding energy of the core electrons can be subtracted out, the valence electron energy change will be a much larger fraction of the total binding energy, and hence much easier to calculate accurately.

Since the atomic wavefunctions are eigenstates of the atomic Hamiltonian, they must all be mutually orthogonal. Since the core states are localized in the vicinity of the nucleus, the valence states must oscillate rapidly in this core region in order to maintain this orthogonality with the core electrons. This rapid

oscillation results in a large kinetic energy for the valence electrons in the core region, which roughly cancels the large potential energy due to the strong Coulomb potential.

It is therefore convenient to attempt to replace the strong Coulomb potential and core electrons by an effective pseudopotential which is much weaker, and replace the valence electron wavefunctions, which oscillate rapidly in the core region, by pseudo-wavefunctions, which vary smoothly in the core region [29, 30](For further details see [31] and also [32, 33] for recent reviews).

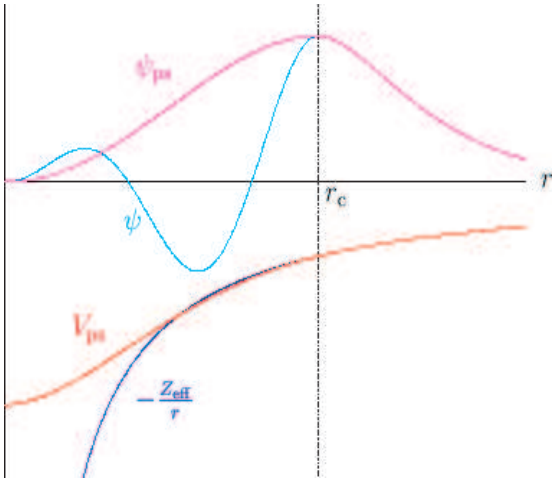

Figure 3.4: Schematic diagram of the relationship between all electron and pseudo potentials, and wavefunctions (Reproduced from University Basel Nanoscience web-page).

In our calculations, we used *Ultrasoft Pseudopotential* which uses a basis set that constitutes of smaller number of planewaves than that of a basis set used by normal pseudopotential.

3.6 Calculation of Conductance Based on Empirical Tight-Binding Method

In order to calculate ballistic conductance G for some of our specific nanowire structures, we used empirical tight-binding method and computer programming developed by Nardelli code. The method used in this code is based on the *Surface Greens Function Matching Formalism* and combines the iterative calculation of transfer matrices with the Landauer formula for the coherent conductance. This section presents a brief outline of the method of calculation.

3.6.1 Green's Function Method

In order to explain conductance calculations of any extended system, such as nanowires in our case, let us consider a system composed of a conductor C connected to two semi-infinite leads, R and L. Fig. 3.5

Figure 3.5: A conductor described by the Hamiltonian H_C , connected to leads L and R, through the coupling matrices h_{LC} and h_{CR} .

The conductance G through a region of interacting electrons is related to the scattering properties of the region itself via the Landauer formula [37]

$$G = \frac{2e^2}{h} T \tag{3.32}$$

In this equation T corresponds to transmission function which is expressed in terms of the coupling of the conductor to the leads and the Green's functions of the conductors [38]

$$T = Tr(\Gamma_L g_C^r \Gamma_R g_C^a) \tag{3.33}$$

where $\Gamma_{[L,R]}$ are functions that describe the coupling of the conductor to the leads and $g_C^{[r,a]}$ are the retarded and advanced Green's functions. The Green's function of the conductor can be computed starting from the following equation for the Green's function of the whole system,

$$(\epsilon - H)g = I \tag{3.34}$$

where $\epsilon = E - i\eta$ with η arbitrarily small, and I is the identity matrix. In here, Green's function of the whole system (g) can be separated into submatrices that corresponds to Green's functions of individual subsystems. Further calculation steps give us, G which is the conductance of conductor C shown in Fig. 3.5

As seen the core of the problem lies in the calculation of the Greens functions of the semi-infinite leads (further details about method for solving this problem can be found at [39]). It should be noted that the solution of Green's functions, requires Hamiltonian matrix, H. This Hamiltonian matrix of the system can be determined by *Empirical Tight-Binding* approach. After constructing H, Green's functions, T transmission function and finally conductance G can be determined by making use of last three equations.

3.6.2 Empirical Tight-Binding Method (ETB)

The empirical or parameterized tight-binding method (ETB) has been employed extensively in the past for the study of semiconductors due to the simplicity of the approach and its ability to describe properties in terms of chemical bonds. This gives the model a more realistic nature as opposed to methods based on weak periodic potentials. The ETB approach is suitable to deal with larger systems compared to the first-principles methods based on plane waves, due to the relatively lower computation time. The ETB method was originally described

by Slater and Koster [40] as an interpolation scheme. It has been developed extensively since then and is now a well established technique to elucidate the electronic structure of solids. Wavefunction of the system can be written as,

$$\Psi(\mathbf{r}) = \sum_{R} e^{i\mathbf{k}\cdot\mathbf{R}}\Phi(\mathbf{r}-\mathbf{R}) \tag{3.35}$$

where $\Phi(\mathbf{r}-\mathbf{R})$ are atomic orbitals (s,p_x, p_y, p_z). The Hamiltonian of the system can be composed of the Hamiltonian, H_{at}, of single atom at the atomic site and all corrections to the atomic potential at the interatomic region $\Delta[U(r)]$ to produce the full periodic potential of the system.

$$H \cong H_{at} + \Delta[U(r)] \tag{3.36}$$

By using this idea, now we can easily construct the Hamiltonian matrix of the system. Normally, each element of Hamiltonian matrix (H_{ij}) is calculated by the following integral,

$$H_{ij} = \int \Psi_i^* H \Psi_j dr^3 \tag{3.37}$$

However this integration is not so simple and requires three dimensional multi center integrals. Therefore, instead of computing the integral, one can represent it by some parameters, i.e tight-binding parameters [41, 42, 43]. Number of these parameters depends on the approximation (i.e first nearest or second nearest neighbor interaction or etc.). In the present thesis up to second nearest neighbor interaction have been taken into account. Therefore 12 different tight-binding parameters $E_s, E_{p_x}, E_{p_y}, E_{p_z}, V_{ss\sigma_1}, V_{ss\sigma_2}, V_{sp\sigma_1}, V_{sp\sigma_2}, V_{pp\sigma_1}, V_{pp\sigma_2}, V_{pp\pi_1}, V_{pp\pi_2}$ must be fitted to the known electronic energy band values (obtained from ab-initio calculations or experimental measurements).

Chapter 4

Results and Discussion

4.1 Motivation

The structure of nanowires itself is important. The stability and periodicity of the atomic structure in one dimension (1D) is of academical and technological interest, because of our limited knowledge in one-dimensional crystallography. Besides, earlier research have argued that at $D \sim \lambda_B$, the conductance G (even the diameter D or size) of nanowires are quantized. Group IV elements, Carbon and Silicon, make semiconductor an insulator in diamond structure, because of their even number of valence electrons appropriate for tetrahedrally directed covalent bonds. Now it's of interest to find their electronic properties when they form very thin nanowires. Possible conductors predicted from these nanowires are expected to be important in microelectronics, which aims at to fabricate device with with dimensions less than 200Å.

4.2 Method of calculations

Our study deals with physical properties of various carbon and silicon nanowire structures from linear chain to hexagonal structure The physical properties comprise optimized atomic structure, electronic Energy bands, bonding and cohesive energy, conductance and metallicity. The binding energy and resulting electronic structure of any stable structure have been calculated by using a first-principles pseudopotential plane wave method within the generalized gradient approximation (GGA) [45].

In our first-principle calculations, we used ultrasoft pseudopotential [46] and plane waves up to an energy cutoff of 330 eV depending on the element. The Brillouin zone (BZ) of the supercell is sampled by (1,1,11) to (1,1,41) **k**-points within the Monkhorst-Pack special **k**–point scheme depending on the element type and the size of (BZ) [47]. Convergence tests have been performed with respect to the energy cutoff and number of k-points. Calculations have been performed in momentum space by using periodically repeating tetragonal supercell with lattice constants, $a_s = b_s \sim 10$ whereby interaction of nearest neighbors in the x and y directions are negligible. The lattice constant along the axis of the nanowire structure coincides with the lattice constant of supercell c_s. In our calculation, we optimized the lattice constant c of the wire by optimizing the lattice constant c_s of the supercell. To enhance the variational freedom in the atomic geometry, we examinedd certain structures in double supercell with $c_s = 2c$.

4.3 Carbon and Silicon Nanowires

4.3.1 Linear Chain C1 and Si1

In order to find the electronic properties of carbon and silicon linear chain (C1 and Si1), we first optimized its structure. This structure is relaxed by selecting the appropriate number of **k**-points and energy cutoff values determined from convergence tests. Number of k-points used in Brillouin zone sampling and energy

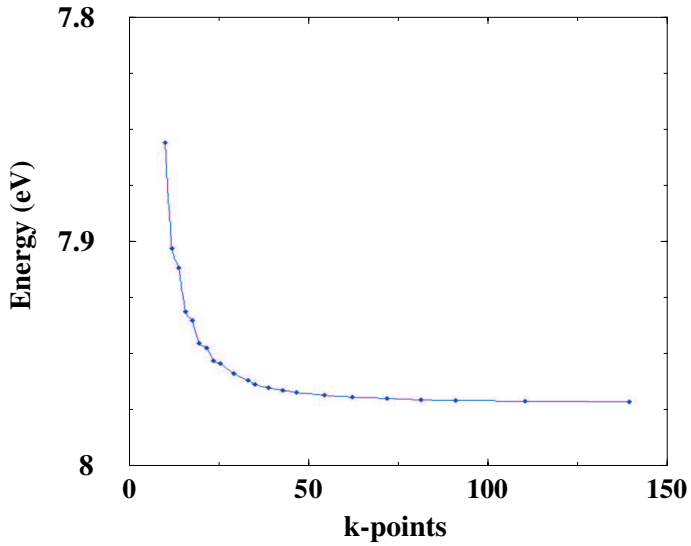

Figure 4.1: Energy versus number of **k**-points graph for carbon.

cutoff values have been determined by convergence tests. Convergence tests have been done by searching the 1 meV energy tolerance between the single-run energy values calculated for each **k**-point (energy cutoff) values. From the total energy versus number of **k**-points (Fig. 4.1) and total energy versus energy cutoff value (Fig. 4.2) graphs for carbon (silicon), it is clear that when 41 **k**-points and 330 eV energy cutoff (37 **k**-points and 210 eV) values are used, we reach 1meV energy tolerance between two single-run energy values.

Thus for our calculations, we have used 41 **k**-points (37 **k**-points) and 330 eV (210 eV) energy cutoff value for carbon (silicon).In our calculations lattice parameters $a_s = b_s$ is taken to be 10 Å as discussed in the previous section. Relaxation process have been done by using program packages. The energy values corresponding to each c_s gives minimum where the system in this configuration is now the most stable structure with respect to the other structures obtained from different c_s values. In order to confirm that the relaxed structure obtained from one unit cell is actually the most stable structure, relaxation is also performed in double unit cell with $c_s = 2c$.

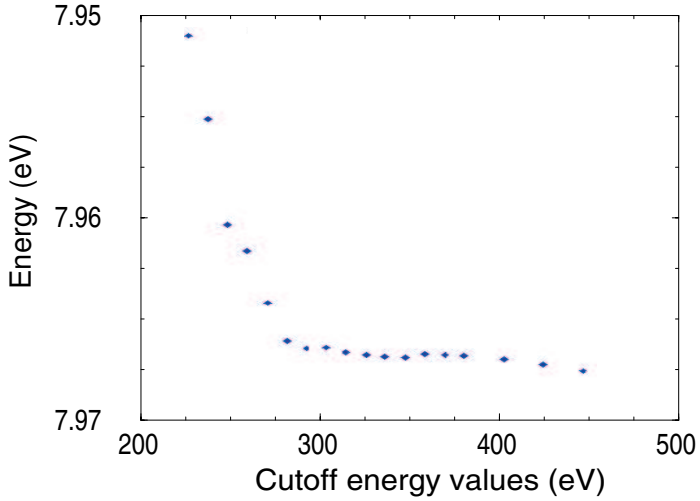

Figure 4.2: Energy versus energy cutoff value graph for carbon.

The optimized structures of C1 and Si1 obtained from first-principle pseudopotential method are shown in Fig. 4.3

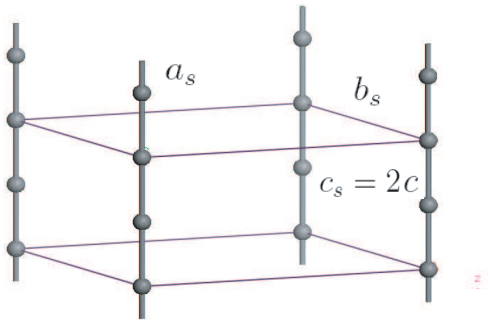

Figure 4.3: Relaxed structure of C_1 and Si_1 in double unit cell with lattice parameters $a_s = b_s = 10$ Å, $c_s = 2 \cdot 1.269$ Å and binding energy $E_{binding} = 8.29$ eV/atom for relaxed C1 structure, and a_s=b_s=10 Å, $c = 2{\cdot}2.217\mathring{A}$, $E_{binding} = 3.45$ eV/atom for Si1 relaxed structure. Supercell is defined by lateral black lines.

Although the atomic structures determined by using Congugate Gradient (CG) method is generally stable, we performed further stability tests of the structures. This way, we excluded the probability the CGA optimized structures corresponds to metastable structure.

Stability test can be applied in various ways. In our work, we chose deforming the structure and looking for the relaxed position of this deformed structure. We deformed C1 and Si1 along the chain (z-direction) and also along x,y directions. By first imposing small deformations in different directions and then by relaxing the structure, we obtained that the deformed structure returns to undeformed one described in Fig. 4.3. This way, we concluded that C1 and Si1 are stable structure. We have been also performing stability tests by calculating the phonon dispersion along Γ-Z direction. Finite temperature quantum molecular dynamics calculations are also used for stability. To this end, first the temperate of the the optimized structure is suddenly raised to T_k $500 < T_k < 1000K^o$ for a short time for ∼ps. Subsequently the structure is cooled quickly. This procedure is called stimulated anneling and conveys useful information about the possible other structures corresponding to neighboring minima in the Born-Oppenheimer surfaces.

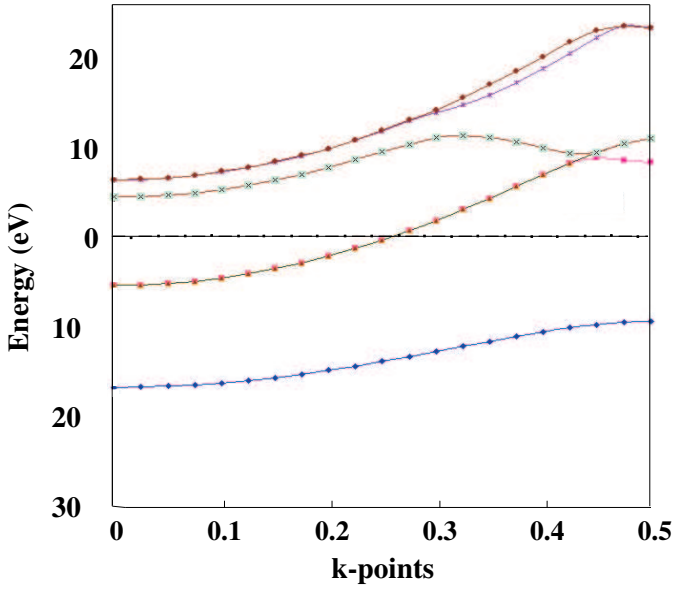

Figure 4.4: Energy band structure of carbon linear chain C1. The Fermi level (E_F) is set at the zero conventionally in this thesis and is shown by dashed dotted line.

The electrical properties of nanowires can be revealed by analyzing their Energy band structure. Energy band structure of C1 and Si1 are similar and shown

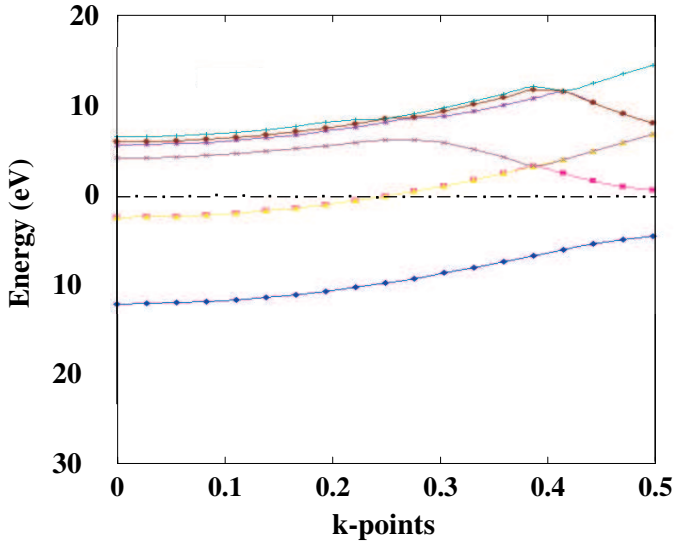

Figure 4.5: Energy band structure of optimized silicon linear chain (Si1). Dashed dotted line corresponds to Fermi level (E_F) set at 0 eV.

in Fig. 4.4 and 4.5. In both cases, the lowest Energy band corresponds to σ band, while Energy band that intersects the Fermi level (E_F) is double degenerate π-band. Upperbands are derived from σ^* and π^* orbitals. From Fig. 4.4 and 4.5 the double degenerate π-band are derived from $2p_x$ and $2p_y$ orbitals intersects the Fermi energy level . Therefore, it can be concluded that optimized C1 and Si1 structures are *metallic*. It is also obvious from density of states of C1 and Si1 (Fig. 4.6 and 4.7), since there is finite density of states at E_F set at 0 eV as a convention in this thesis.

Since there is one two-fold degenerate Energy band intersecting E_F in Fig. 4.4 and Fig. 4.5, one predicts that the conductance of the linear chain is about $2G_0$ ($G_0 = 2e^2/h$). Conductance calculations have been carried out by using empirical tight-binding method (ETM) discussed in Chapter 3.6.2. The Hamiltonian matrix constructed within empirical parameters, determined by fitting tight-binding band shown in Fig. 4.8 to first-principle bands in Fig. 4.5.

The conductance of C1 is determined by the Band structure shown in Fig. 4.4. For an infinite, perfect C1 structure electrons are transported ballistically without

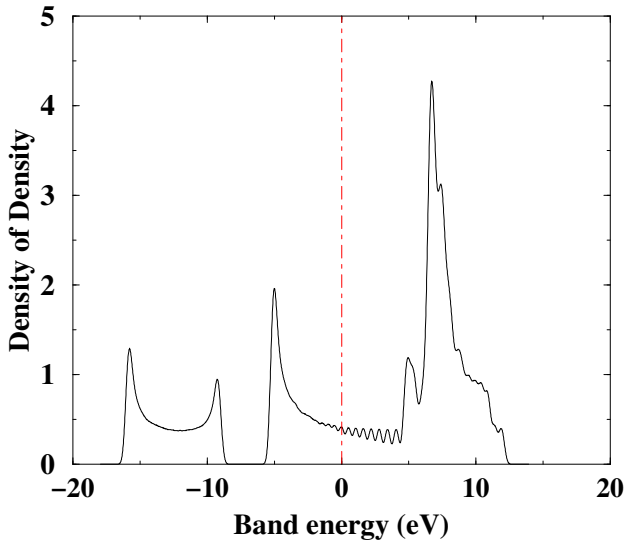

Figure 4.6: Density of states (DOS) of carbon linear chain described in Fig. 4.3. Dashed dotted lines corresponds to Fermi level E_F set at 0 eV. The claim is metallic owing to the finite DOS at E_F.

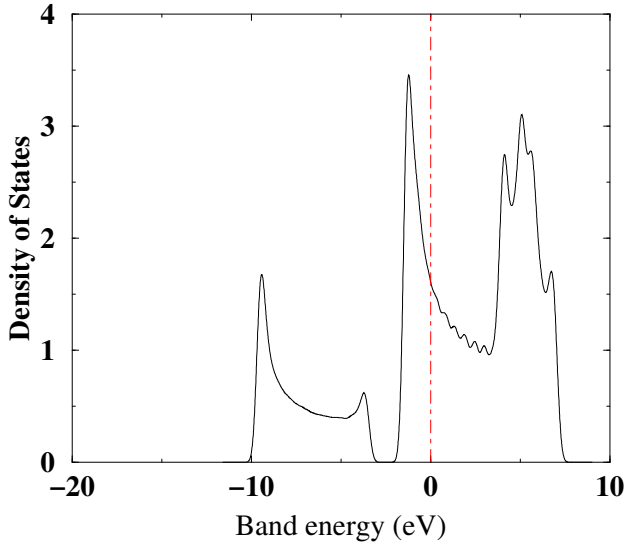

Figure 4.7: Density of states of Silicon linear chain (Si1) described in Fig. 4.3. Dashed dotted lines corresponds to Fermi level E_F set at 0 eV. Since there is finite density of states at E_F, Si1 structure is metallic.

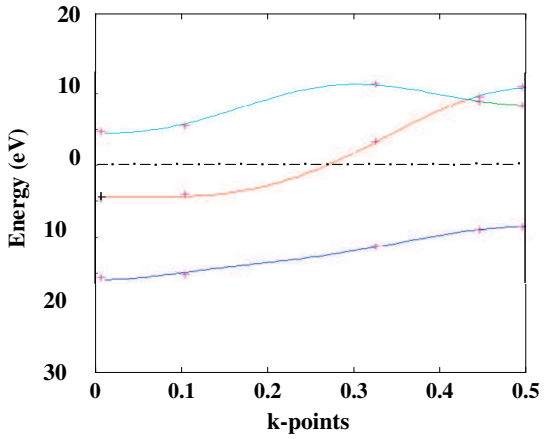

Figure 4.8: The band-structure of C1 calculated by emprical tight-binding method (ETB) fitted to first-principle band structure shown in Fig. 4.4. + indicate the first-principle band energies. E_F shown by dashed dotted line set at 0 eV. Tight-binding parameters are: $E_s = -17.096$ eV,$E_{p1} = -3.545$ eV,$E_{p2} = 3.282$ eV,$V_{ss\sigma} = -1.559$ eV,$V_{sp\sigma} = 1.463$ eV,$V_{pp\sigma} = -1.276$ eV,$V_{pp\pi} = -3.827$ eV,$V_{ss\sigma} = 0.256$ eV,$V_{sp\sigma} = 0.956$ eV,$V_{pp\sigma} = -1.228$ eV,$V_{ss\sigma} = -0.841$ eV, where the last four parameters obtained from second nearest interaction.

any scattering. Under these circumstances the mean free path, $l_m \sim \infty$. Under a finite bias voltage V_b, the conductance of G of C1 are calculated by the tight-binding Green's function (TBGF) technique using program developed by Nardelli. In this calculation of Green's function the tight-binding band structure of C1 is essential to this and the ab-initio band structure of C1 in Fig. 4.4 is fitted to a tight-binding band shown in Fig. 4.8. In Fig. 4.8 the tight-binding band energies are compared with first-principles band energies.

The conductance G versus V_b curve calculated for C1 by the TBGF method is shown in Fig. 4.9. At V_b=0, the G(V_b)=2($2e^2/h$) since double degenerate π-band crosses the Fermi level hence makes two current transporting states available for conductance.

Similar calculation have been also carried out for Si1, and hence conductance G versus V_b curve calculated by using the TBGF method is shown in Fig. 4.10. Same interpretations for C1 structure are also valid for silicon linear chain Si1.

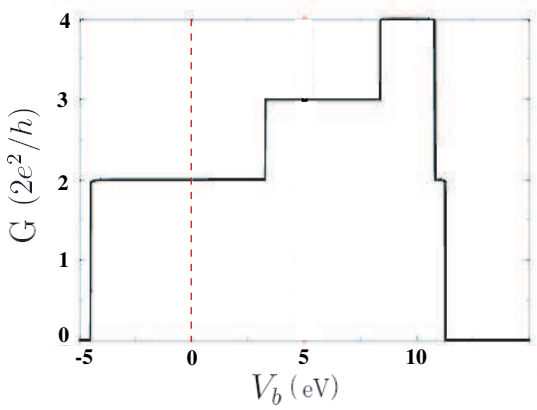

Figure 4.9: Ballistic quantum conductance G versus bias voltage V_b of carbon linear chain. Vertical dashed line indicates the Fermi level. At Fermi level, conductance of carbon linear chain is $2G_0$ where $G_0 = 2e^2h$

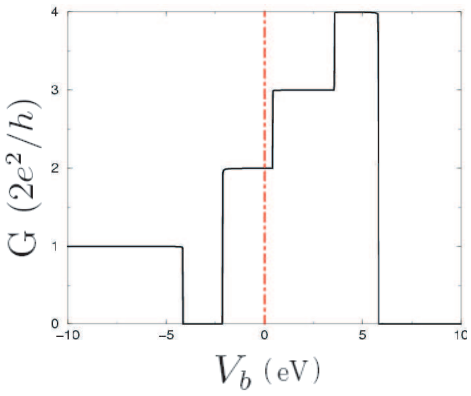

Figure 4.10: Quantum ballistic conductance G versus bias voltage V_b for silicon linear chain (Si1). Vertical line indicates the Fermi level. At E_F, conductance of silicon linear chain is $2G_0$.

4.3.2 Planar Triangular (C2 and Si2)

In this structure, all (C or Si) atom forming the trianglular structure lie in the same plane as shown in Fig 4.11. Accordingly the supercell comprises two atoms. In order to find the electronic properties of C2 and Si2 (Fig. 4.11(a)), we first optimized these structures. Si2 structure is relaxed by selecting appropriate number of **k**-points (37) and energy cutoff value (210 eV) determined from convergence tests discussed in Chapter 4.3.1.

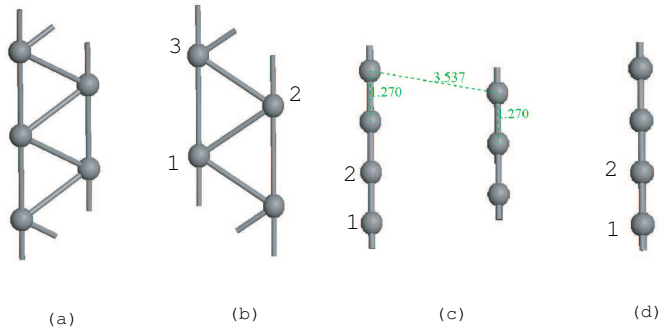

Figure 4.11: (a) Initial structure of C2 and Si2 with initial angle 60^o (b) Optimized structure of Si2 with binding energy $E_{binding} = 4.19eV/atom$, bond distances 1-2=2.38Å, 2-3=2.38Å, 1-3=2.45Åand angle $\widehat{123} = 62^o$ (c) Relaxed configuration of C2 structure which corresponds to 1^{st} minimum in Fig. 4.14. Since C2 structure is compressed in z direction, it favors to construct two non-interacting carbon linear chains with distance between them 3.5Åand C-C bond length 1-2=1.27Å(d) Relaxed structure at 2^{nd} minimum of Fig. 4.14 Since the lattice parameter in z direction, $c_s = 2.55\mathring{A}$, C atoms form a linear chain with C-C distance 1.27Å

After optimization, the structure of Si2 has changed to the equilateral triangle to an isosceles triangle with the opex angle of 62^o. In order to confirm that this structure is stable, we performed stability tests by deforming the structure and relaxing this deformed one. The structure is deformed by changing the angle $\widehat{123}$ and by displacing atoms labelled by 2 and 3 by finite distance of order 0.1Å-0.3Å. Stability tests reveal that the relaxed structure of Si2 is stable, since deformed structure returns to its initial position.

Energy band structure of this stable structure of Si2 is shown in Fig. 4.12.

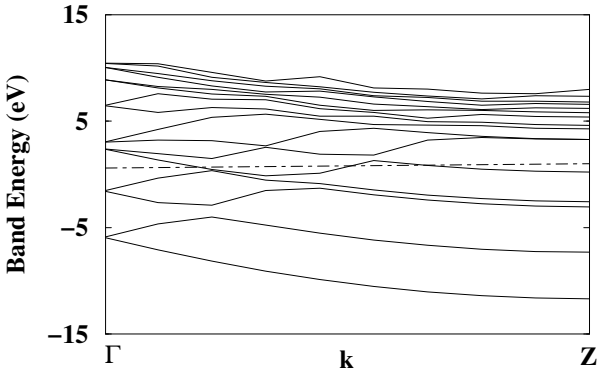

Figure 4.12: Energy band structure of optimized Si2 structure. There are four bands that intersect the Fermi level shown by a thick line.

Since there are four bands intersecting the Fermi level, this structure is metallic. This is also clear from DOS of Si2 structure, since there is finite density of states at E_F. One can estimate the quantum ballistic conductance of the stable structure near E_F from the total number of bands that intersect E_F. In our case, conductance is estimated to be $4G_0$. Owing to the difficulties of fitting of complex band structure we did not perform conductance calculations.

The optimized structure of C2 obtained from first-principle pseudopotential method has changed to the linear chain (C1) structure. Energy-lattice parameter versus c_s graph, which is obtained by calculating total energy corresponding to different c_s's (see Fig. 4.14) give two global minimum at $c_s = 1.27$Å and $c_s = 2.55$Å. The relaxed structures at these two minima corresponds to same linear chain and these are illustrated in Fig. 4.11(c,d).

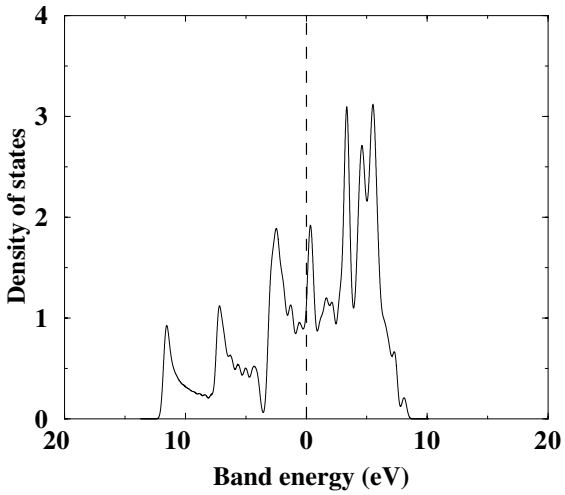

Figure 4.13: Calculated DOS of Si2 structure. There is finite density of states at the Fermi level set at 0 eV, acoordingly this structure is metallic.

4.3.3 Zigzag Structure (C_3 and Si_3)

The zigzag structure can be described by isosceles triangular structure with large apex angle ($> 100^o$). It has two atoms in the supercell.

Silicon zigzag structure Si3 and carbon zigzag structure C3 shown in Fig. 4.15 are optimized. The optimized structure of Si3 obtained from the pseudopotential method is illustrated in Fig. 4.15.

In the stability tests, Si3 is first deformed and subsequently is relaxed. The displaced atoms have returned to its initial positions. Electronic properties of Si3 is studied by analyzing the band structure illustrated in Fig. 4.16. Since there is no bands intersecting the Fermi level, this structure is semiconductor with band gap $E_{gap} = 0.3eV$.

Similar calculation steps also done for C3 structure, and we found that C3 is not a stable structure, since this structure relaxes to C1.

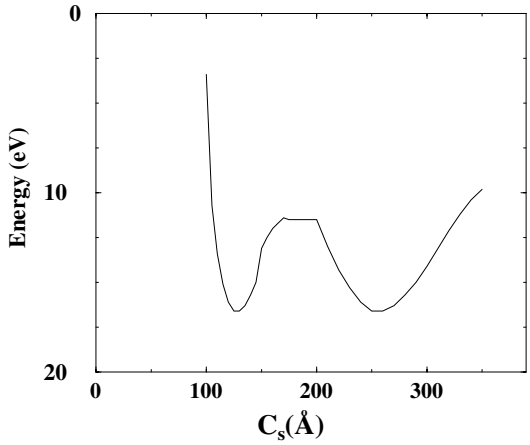

Figure 4.14: Total energy versus lattice constant c_s for carbon triangular and zigzag structure. There are two minima at c_s=1.27Å and c_s=2.55Å. Relaxed structures of 1^{st} and 2^{nd} minimum are identical.

Figure 4.15: Initial zigzag structure with $\widehat{123} = 120^o$. The optimized Si3 has zigzag structure with bond lengths $d_{12} = d_{23} = 2.18\mathring{A}$, $d_{13} = 3.74\mathring{A}$, angle $\widehat{123} = 118.22^o$, and binding energy $E_{binding} = 3.85eV$. C3 structure disintegrated after optimization.

4.3.4 Dumbell Structure (C_4 and Si_4)

Dumbell structure is made by perpendicular Si_2 (C_2) molecules and includes four atoms in the unit cell. Carbon and Silicon dumbell structure described in Fig. 4.17, is relaxed. Similar to the relaxation of carbon zigzag structure, C4 structure has changed to linear chain structure after relaxation as shown in Fig. 4.17(b).

With appropriate parameters, Si4 structure is optimized to dumbell structure with structure parameters indicated in Fig. 4.17(a). In the tests of stability we first deformed this structure by rotating each C-C pair, i.e 1-2 or 3-4 in Fig 4.17 by

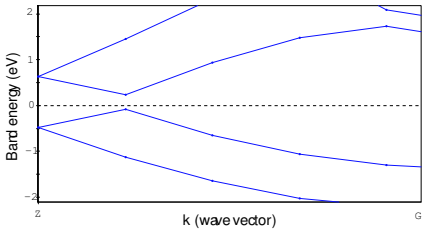

Figure 4.16: Energy band structure of Si3. This structure is semiconductor with Energy band gap $E_{gap} = 0.3eV$.

a finite angle ϕ and by displacing the carbon atoms from its initial positions.Upon relaxation displaced atoms have returned to their original positions indicating the fact that the Si4 structure is stable.

Energy band structure of this stable structure is illustrated in Fig. 4.18. Since there is three bands intersecting the Fermi level, this structure is metallic and one can estimate the conductance to be $3G_0$. DOS of Si4 is illustrated in Fig. 4.19. The finite state density of E_F shows the metallicity of the nanowire.

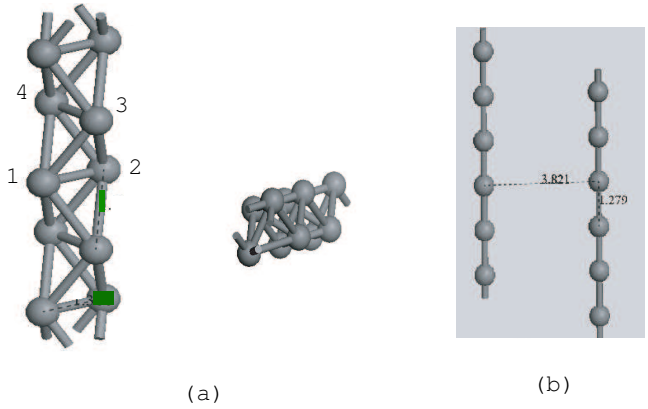

Figure 4.17: (a) Carbon and silicon dumbell structures shown in different angles. This is also optimized structure of Si4 with binding energy $E_{binding} = 4.58$ eV/atom and bond lengths $d_{12} = d_{34} = 2.6\mathring{A}$, $d_{23} = d_{14} = 2.45\mathring{A}$, $d_{13} = d_{24} = 2.46\mathring{A}$ (b) Structure obtained after the relaxation of carbon dumbell structure, where two noninteracting carbon linear chains separated by 3.821Å is generated with $d_{c-c} = 1.259\mathring{A}$ distance.

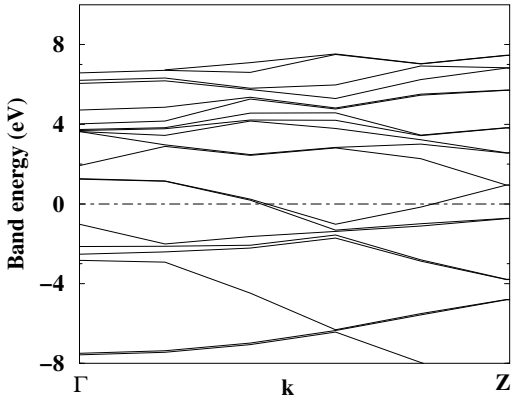

Figure 4.18: Band structure near Fermi level E_F. There are three bands that intersect E_F, therefore the structure is metallic with conductance G=$3G_0$.

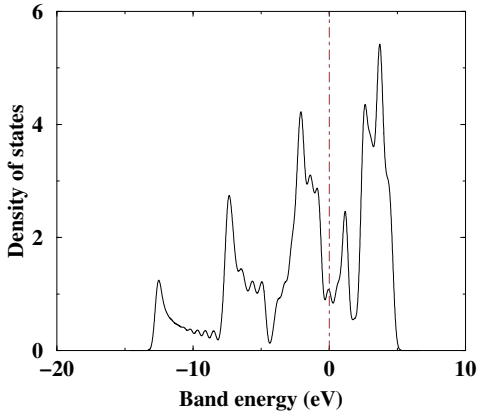

Figure 4.19: Density of states of Si4. It is clear that the stable structure is metallic, since there is finite DOS at Fermi level.

4.3.5 Triangular Structure (C_{T1}, C_{T2} and Si_{T1}, Si_{T2})

In this category, the triangles of atoms are perpendicular to the axis of the wire which passes through their centers. We consider two types of structures. Namely top to top triangular structures (C_{T1} and Si_{T1}) and staggered triangular structures (C_{T2} and Si_{T2}). Those structures are relaxed in single and double supercell. Upon relaxation, we found that C_{T1} as well as C_{T2} are not stable.

Our structure optimization calculations yield stable Si_{T1} structure, with a binding energy $E_{binding} = 4.58$ eV/atom. In the tests of stability, we first deformed the structure by rotating one triangle around the axis by a finite angle relative to adjacent. In the Energy band structure of Si_{T1} illustrated in Fig. 4.21 four bands intersecting E_F attribute metallic properties to the nanowire. Accordingly the quantized ballistic conductance is estimated to be $G = 4G_0$. The calculated density of states shown in Fig. 4.22 has very high density of states at E_F. This situation indicates the possibility that Si_{T1} can be a superconductor.

Similar to Si_{T1}, Si_{T2} has satisfied the stability tests and has been found to be metallic with $3G_0$.

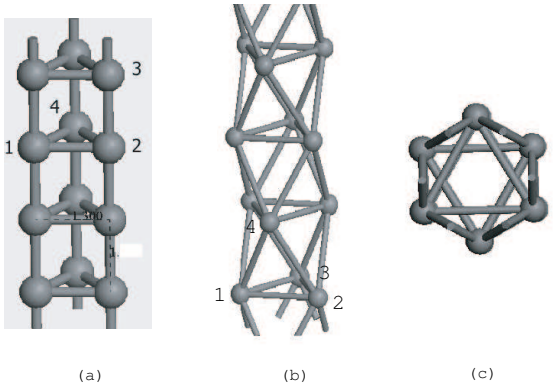

Figure 4.20: (a)Initial C_{T1} and Si_{T1} structure. After optimization C_{T1} system is disintegrated, while Si_{T1} gives stable top to top triangular structure with binding energy $E_{binding} = 4.58$ eV/atom and bond lengths $d_{1-2} \sim d_{1-4} \sim d_{2-4} = 2.41\mathring{A}$, $d_{2-3} = 2.37\mathring{A}$. (b) Initial C_{T2} and Si_{T2} structure. After optimization C_{T2} system is disintegrated, while Si_{T2} gives stable staggered triangular structure with binding energy $E_{binding} = 4.55$ eV/atom and bond lengths $d_{1-2} \sim d_{1-3} \sim d_{2-3} \sim d_{4-5} = 2.42\mathring{A}$, $d_{2-3} = 2.37\mathring{A}$, $d_{1-4} \sim d_{2-4} = 2.58\mathring{A}$. (c) Top view of Si_{T2} and C_{T2} structure.

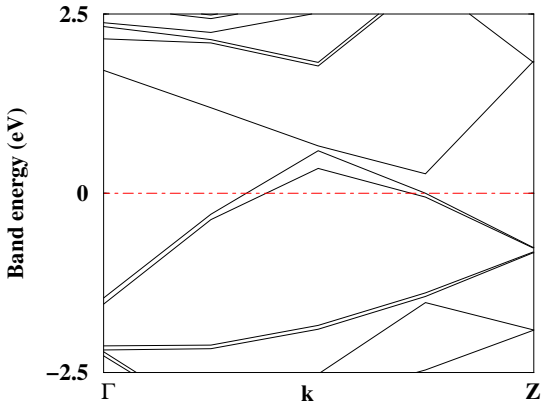

Figure 4.21: Energy band structure of relaxed Si_{T1} structure. There are four bands that cross E_F. The structure is metallic with conductance $4G_0$.

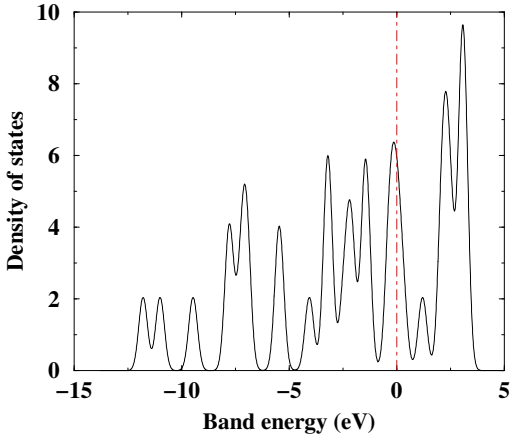

Figure 4.22: DOS of $Si_{T1}$with finite state density at E_F.

4.3.6 Triangular Structure with Linear Chain

This type of structure is similar to ones described in section 4.3.5, except a linear chain which passes through the centers of triangles. Thus the linear chain coincides with the axis of the nanowire. Silicon top to top triangular with linear chain (Si_{T3}) and silicon staggered triangular with linear chain (Si_{T4}) structures are optimized. The optimized structures of Si_{T3} and Si_{T4} are illustrated in Fig. 4.23. In order to test whether the structures obtained by CGA are stable or not, we performed stability tests. Stability tests have revealed that the optimized structures are stable, since these structures returns to their initial undeformed position after deformation.

Electrical properties of optimized Si_{T3} and Si_{T4} can be summarized as follows; Since there are bands crossing E_F as in Si_{T1} in Fig. 4.21, both of these structures are metallic. In the Energy band structure of Si_{T3} (Si_{T4}) there are six (three) bands that intersect E_F, hence one expects $6G_0$ ($3G_0$) conductance for this structure.

Similar calculations have been performed for C_{T3} and C_{T4}, and both of these structures are disintegrated after relaxation process.

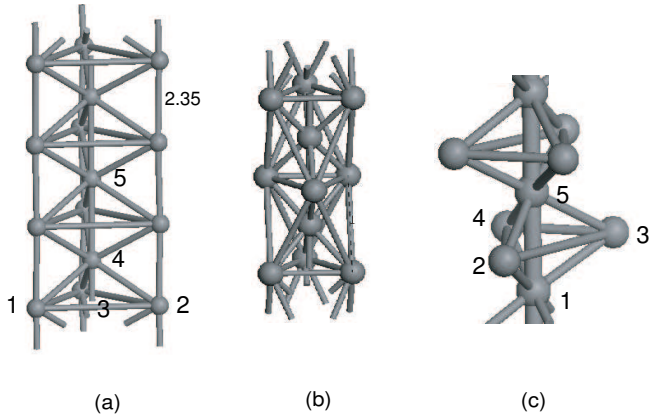

Figure 4.23: (a) Initial structure of C_{T3} and Si_{T3} structure. C_{T3} structure disintegrated after optimization, while Si_{T3} relaxed to top to top triangle with linear chain with binding energy $E_{binding}$ = 4.34 eV/atom and bond lengths $d_{1-2} = 3.55\mathring{A}$, $d_{1-3} = 3.93\mathring{A}$, $d_{2-3} = 3.84\mathring{A}$,$d_{4-5} = 2.35$ (b) Initial structures of C_{T4} and Si_{T4}. C_{T4} disintegrated after optimization. (c) Relaxed structure of Si_{T4} with $E_{binding}$ = 4.47 eV/atom and bond lengths $d_{15} = 2.3\mathring{A}$, $d_{23} = d_{24} = 4.15\mathring{A}$, $d_{34} = 2.56\mathring{A}$

4.3.7 Triangle+Single Atom+Single Atom (C_{T5})

In this structure there are two atoms in the axis of the wire between two adjacent top to top triangles. In order to find the detailed electronic properties of C_{T5} structure described in Fig. 4.24(a), we first optimized the atomic positions. The optimized structure of C_{T5} is depicted in Fig. 4.24(b). We performed stability tests in which structure is deformed, by imposing small deformations in different directions to two single atoms and staggering triangle by finite angle $\Delta\phi$, and then the deformed structure is optimized. Since the deformed structures have returned to their original optimized structures in Fig. 4.24(b) upon relaxation, it is concluded that C_{T5} structure is stable.

Energy band structure of the relaxed structure is shown in Fig 4.25. Energy band structure shows that this stable structure is *insulator* with $E_{gap} = 3.4eV$. This situation is also obvious from density of states graph illustrated in Fig. 4.26.

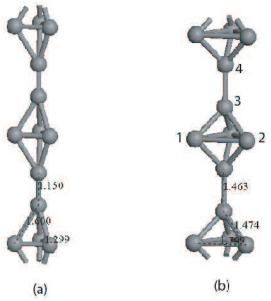

Figure 4.24: (a) Initial C_{T5} structure. (b) Relaxed C_{T5} structure with $E_{binding}$ = 7.42 eV/atom and bond lengths $d_{12} = 1.80$Å, $d_{13} = 1.47$Å, $d_{34} = 1.46$Å.

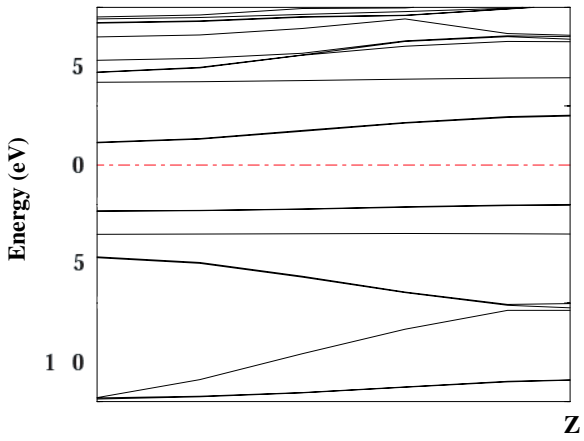

Figure 4.25: Energy band structure of the C_{T5} structure. C_{T5} is insulator owing to huge band gap of $E_{gap} = 3.4eV$.

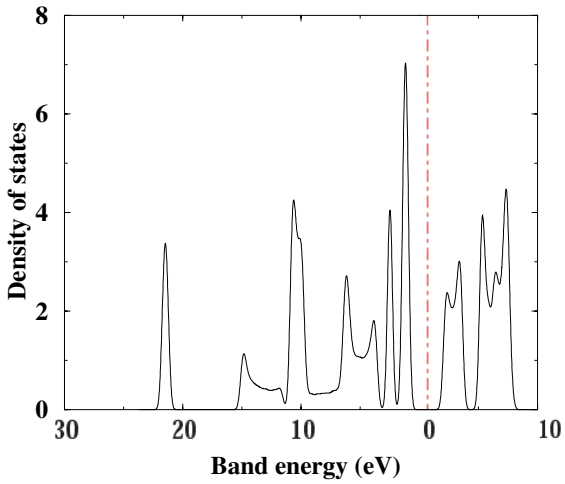

Figure 4.26: Calculated DOS of C_{T5} structure.

4.3.8 Pentagonal structures

This structure consists of top to top and staggered pentagons perpendicular to the axis of nanowire. Both top to top (C_{p1}) and staggered (C_{p2}) structure of carbon have been optimized. Optimized structure have been found in the top to opt pentagonal structure. The binding energy $E_{binding}$ = 7.46 eV/atom and bond lengths $d_{12} = d_{23} = 1.55\mathring{A}$, $d_{34} = 1.59\mathring{A}$ (Fig. 4.27). The stability of the optimized structure confirmed by performing stability tests.

Energy-band structure reveals that this structure is *semiconductor* with 0.75eV band gap. This is also clear from density of states shown in Fig. 4.29

Similar calculations have been done for the silicon pentagonal structures. After optimization top to top pentagon (Si_{P1}), relaxed to top to top pentagon with binding energy $E_{binding}$ = 4.78 eV/atom and bond lengths $d_{12} = d_{23} = 2.36\mathring{A}$, $d_{34} = 2.39\mathring{A}$. Optimization of staggered pentagon (Si_{P2}) give staggered structure with $E_{binding}$ = 4.67 eV/atom in Fig. 4.27. In this structure distance between each pentagon plane is 1.96Å. Stability tests for Si_{P1} and Si_{P2} confirmed that, both of these structures are stable.

The calculated energy band structure of Si_{p1} shown in Fig. 4.30 suggests

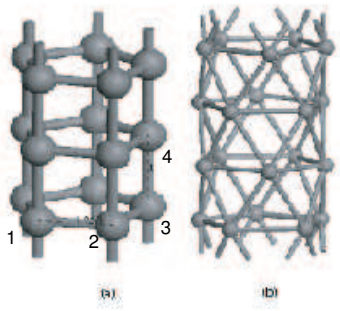

Figure 4.27: (a) Initial structure of pentagonal structures C_{P1} and Si_{P1}. After optimization both of these structures give top to top pentagon structure with binding energies $E_{binding}$ = 7.46 eV/atom for C_{P1} and $E_{binding}$ = 4.78 eV/atom for Si_{P1}.(b) Initial structure of C_{P2} and Si_{P2}. C_{P2} relaxed to C_{P1}, while Si_{P2} gives 36^o staggered pentagon with binding energy $E_{binding}$ = 4.67 eV/atom

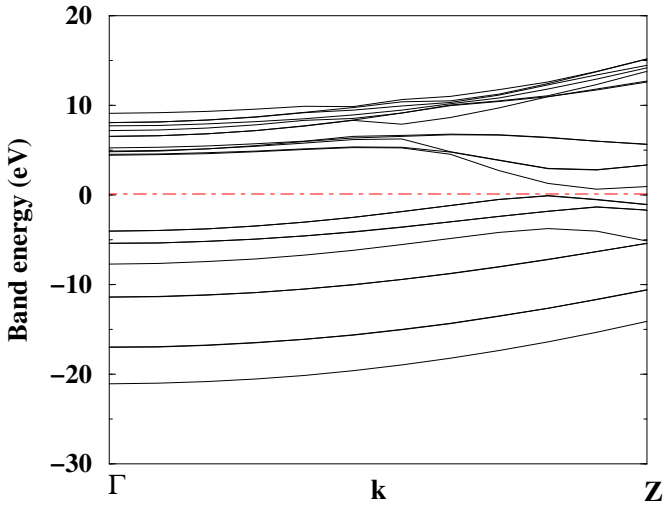

Figure 4.28: (a)Energy band structure of optimized structures of C_{P1}. (b) Enlarged view depicts the band structure near the Fermi level at $T = 0K^o$ with 0.75 eV band gap. Hence the relaxed structure is a semiconductor

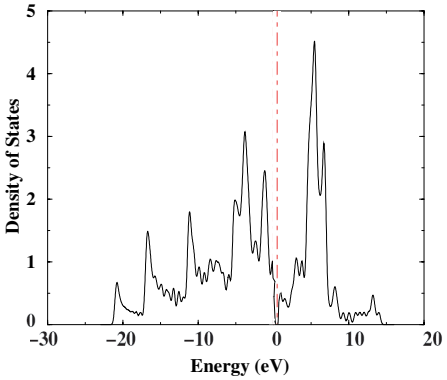

Figure 4.29: Density of states of relaxed structure of C_{P1}. State density vanishes at E_F.

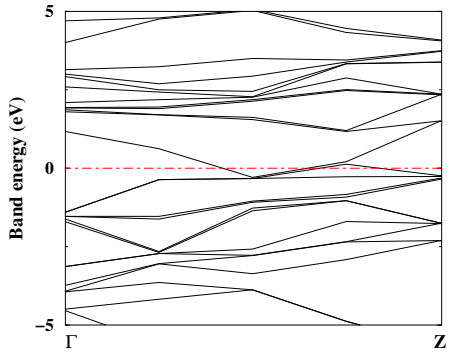

Figure 4.30: Energy band structure of Si_{P1} structure. There are four bands crossing the Fermi level E_F.

metallic properties. Since there are four bands intersecting E_F the conductance of this structure is expected to be $4G_0$. Band structure and density of states of Si_{P2} structure is similar to that of Si_{P1} except that there are three bands crossing the Fermi level instead of four and state density at Fermi level is less than the value for Si_{P2} at E_F.

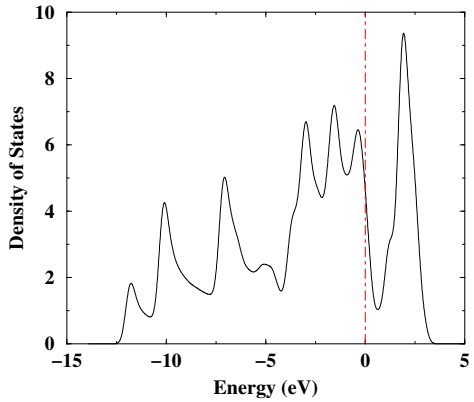

Figure 4.31: Total density of states for Si_{P1} structure. Finite density of states at Fermi level indicates that the structure is metallic.

4.3.9 Pentagonal Structures with Linear Chain

This structure differs from the pentagonal structure in the previous section by the inclusion of atomic chain (having single atom between the pentagons) coinciding with the axis of the wire.

Silicon top to top pentagon with linear chain structure (Si_{P3}) and staggered pentagon with linear chain (Si_{P4}) structures are described in Fig. 4.32. The latter structure consists of two staggered pentagons where one pentagon is rotated by an angle $\phi = 36^o$ with respect to the other pentagon in the supercell and one single atom placed between these two pentagon. Upon optimization we found that both structures Si_{P3} and Si_{P4} are stable with binding energy $E_{binding} = 4.65eV$ and $E_{binding} = 4.60eV$ respectively.

Electronic properties of Si_{P3} and Si_{P4} are comparable to that of Si_{P1}. Since there are six bands crossing the Fermi level for Si_{P3} and four bands for Si_{P4}, these structures are metallic with $6G_0$ and $4G_0$ conductance values. Energy band structures and density of states are similar to that of Si_{P1} structure shown by Fig. 4.30 and Fig. 4.31. C_{P3} and C_{P4} are disintegrated after optimization.

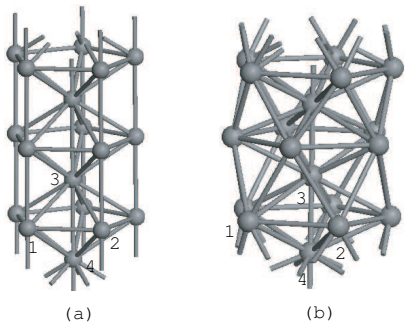

Figure 4.32: (a) Initial C_{P3} and Si_{P3} structures. After optimization Si_{P3} relaxed to top to top pentagonal structure with linear chain structure with $E_{binding} = 4.65eV$ and bond lengths $d_{12} = 2.47\mathring{A}$, $d_{34} = 2.7\mathring{A}$, while C_{P3} disintegrates. (b) Staggered pentagonal, C_{P4} and Si_{P4}, structures. Similarly, the C_{p4} structure has disintegrated after relaxation process. Si_{P4} has changed to staggered pentagon with linear chain with binding energy $E_{binding} = 4.60eV$ and bond lengths $d_{12} = 2.51\mathring{A}$, $d_{34} = 2.78\mathring{A}$

4.3.10 Hexagonal Structures

Similar to the pentagonal structure, top to top or staggered hexagons are perpendicular to the axis of the wire. After optimization, both carbon top to top hexagon (C_{H1}) and staggered hexagon (C_{H2}) where one hexagon is staggered by $\pi/6$ relative to adjacent ones shown (Fig. 4.33) are relaxed to top to top hexagon structure, with binding energy $E_{binding} = 7.42$ eV/atom and same distances $d_{12} = d_{23} = 1.55\mathring{A}$, $d_{34} = 1.60\mathring{A}$.

Band structure of the resulting relaxed structure presented in Fig. 4.34 indicates that the structure is *semiconductor* with band gap $E_{gap} = 0.6eV$. This is also clear from the calculated density of states in Fig. 4.35.

Similar calculations have been performed for top to top hexagon (Si_{H1}) and staggered hexagon structure (Si_{H2}) structures.Both Si_{H1} and Si_{H2} kept their structurel form after relaxation with binding energies $E_{binding} = 4.72eV/atom$ and $E_{binding} = 4.63eV/atom$. Bond lengths were $d_{12} = d_{23} = 2.35\mathring{A}$, $d_{34} = 2.38\mathring{A}$ for Si_{H1} and $d_{12} = 2.49\mathring{A}$, $d_{23} = 2.30\mathring{A}$, $d_{34} = 2.39\mathring{A}$ for Si_{H2}. We performed

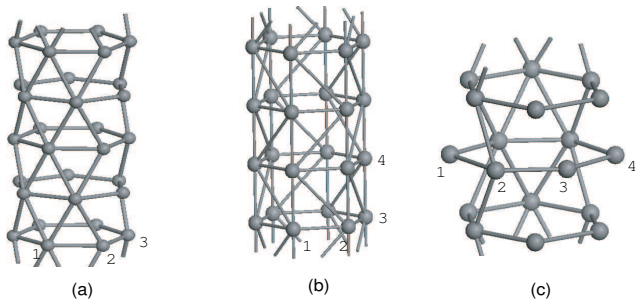

Figure 4.33: (a) Staggered hexagon structure. One hexagon is staggered by amount of $\pi/12$ with respect to the other hexagon. (b) Top to top hexagon structure

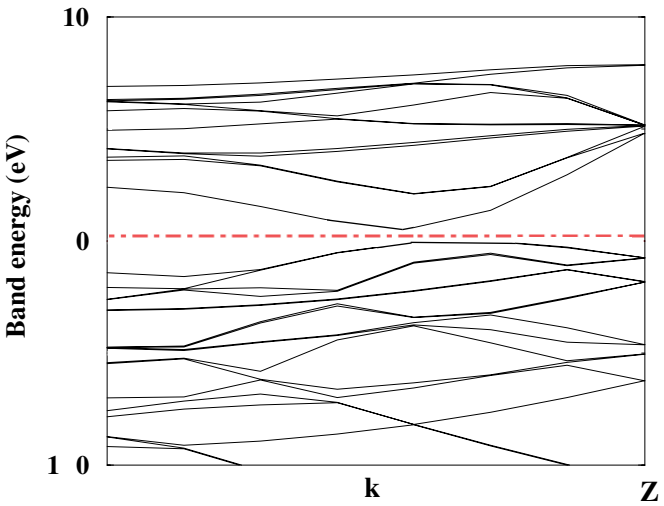

Figure 4.34: Band structure of stable carbon top to top hexagon structure C_{H1}. The structure is semiconductor with band gap $E_{gap} = 0.6eV$.

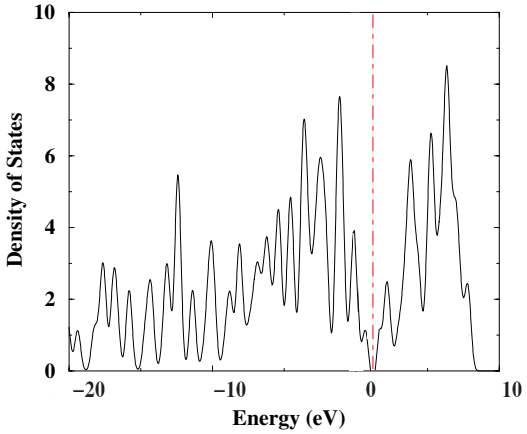

Figure 4.35: Calculated total density of states of C_{H1}.

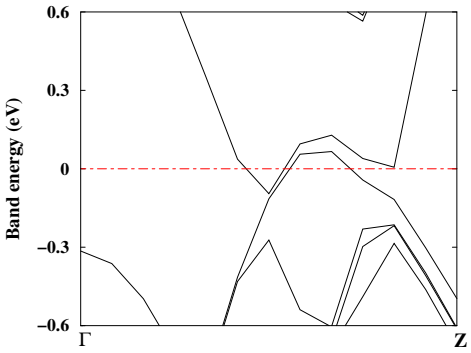

Figure 4.36: Energy band structure of Si_{H1} structure.There are four bands intersecting the Fermi level represented by dashed lines.

stability tests by deforming these structures in such a way that one hexagon is staggered by an angle ϕ with respect to the other hexagon in the same supercell. Stability tests confirmed that structures obtained from CG results are stable.

Electrical properties of Si_{H1} can be determined from its Energy band structure. Since there are four bands crossing the Fermi level (Fig. 4.36) leading to a finite density of states at E_F as shown in Fig. 4.37, Si_{H1} is a good metal. One can estimate $4G_0$ quantum ballistic conductance for the structure. Electrical properties of Si_{H2} is similar to the Si_{H1}, except that three bands are crossing E_F.

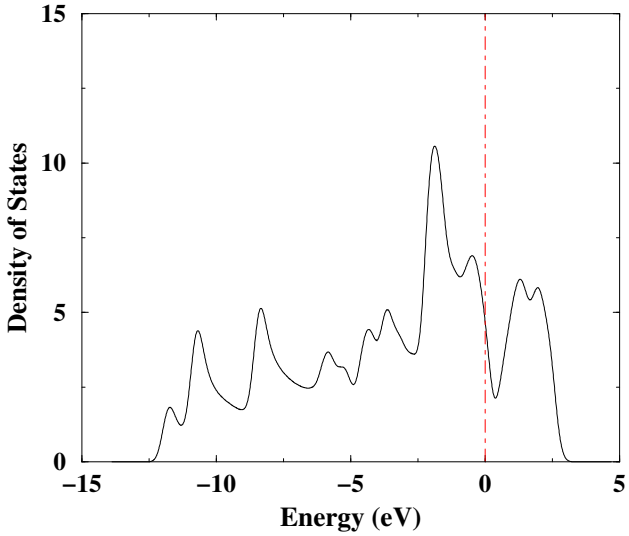

Figure 4.37: Calculated density of states (DOS) of Si_{H1}.

4.3.11 Hexagonal Structures with Linear Chain

This structure is similar to hexagonal structures in the previous section, except that an axial atomic chain, passes through the centers of hexagons. First we consider silicon top to top hexagon with linear chain (Si_{H3}) and staggered hexagon with linear chain (Si_{H4}). Upon optimizing Si_{H3} (Si_{H4}) remained top to top (staggered) hexagon with binding energy $E_{binding} = 4.75eV$ ($E_{binding} = 4.65eV$) and bond distances $d_{12} = 2.35\mathring{A}$ ($d_{12} = d_{25} = 2.48\mathring{A}$, $d_{34} = 2.3\mathring{A}$). Stability tests have shown that Si_{H3} and Si_{H4} structures are stable.

Energy band structure and DOS of Si_{H3} and Si_{H4} are similar to that of Si_{H1} structure. Both structures are metallic with $6G_0$ for Si_{H4} and $4G_0$ conductance for Si_{H3} structure.

Similar calculations were performed for carbon top to top hexagon with linear chain (C_{H3}) and carbon staggered hexagon with linear chain (C_{H4}). After relaxation, both of these structures are disintegrated.

4.3.12 Hexagon+Hexagon+Triangle Structure (C_{H5} and Si_{H5})

This structure consists of two hexagons and one triangle and is reminiscent of a diamond along the [111] direction. Optimized carbon hexagon+hexagon+triangle structure (C_{H5}) is stable and has binding energy $E_{binding} = 7.42$ eV/atom. Band structure of the optimized stable structure is illustrated in Fig. 4.40. Since there is one two-fold degenerate band that intersects E_F, stable C_{H5} structure is metallic, this is also clear from the calculated DOS in Fig. 4.41. From the number of bands that intersect Fermi level, one can predict that quantum ballistic conductance of the system is $2G_0$.

Similar optimization calculations on silicon hexagon+hexagon+triangle (Si_{H5}) structure, resulted in disintegration.

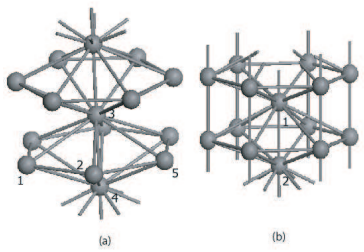

Figure 4.38: (a) Staggered hexagon with linear chain structure where one hexagon is rotated in its plane by an angle $\phi = 30^o$ relative to the adjacent hexagons. (b) Top to top hexagon with linear chain structure.

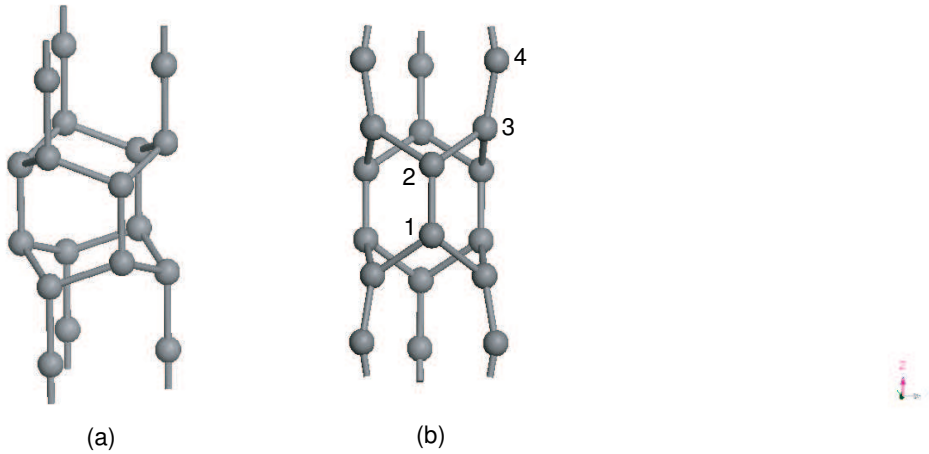

Figure 4.39: (a) Initial C_{H5} and Si_{H5} structures. This structure consists of two buckled hexagons and one triangle (b) The optimized structure of C_{H5} with $E_{binding} = 7.99eV$ and bond lengths $d_{12} = 1.35\mathring{A}$, $d_{23} = 1.51\mathring{A}$, $d_{34} = 1.33\mathring{A}$. This structure is similar to the initial one, except that the bond lengths between the atoms of triangular layer are now stretched.

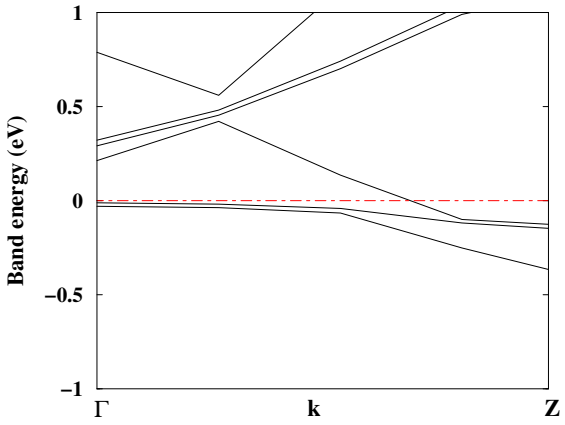

Figure 4.40: (a) Energy band structure of stable C_{H5} structure. There is one two-fold degenerate band which intersects the Fermi level. Therefore the structure is metallic with conductance $2G_0$.

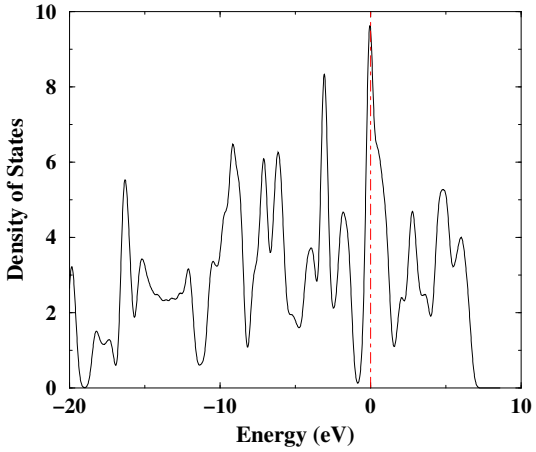

Figure 4.41: Calculated DOS of C_H5

4.3.13 Buckled Hexagon and Triangle Based Structure(C_{H6} and Si_{H6})

This structure consists of two triangle where one triangle 180^o staggered with respect to the other triangle and two buckled hexagon. Each buckled hexagon structure can be envisioned as composed of two 180^o staggered triangle with a 0.51Å spacing. Carbon triangle+ buckled hexagon+staggered triangle+buckled hexagon structure C_{H6} in Fig. 4.42 (a) is relaxed. The optimized structure of C_{H6} is depicted in Fig. 4.42 (b), with binding energy $E_{binding} = 7.93$ eV/atom. The stability tests of the C_{H6} structure is further performed by displacing atoms from equilibrium positions. Upon relaxing displaced atoms have returned to their original positions.

Electronic properties of this stable structure are summarized in Fig. 4.43. Calculated band structure and density of states indicate that this structure is *metallic*. We can estimate conductance of the stable structure near Fermi level from the number of crossing bands. Since there are three bands that intersect Fermi level, we can say that the conductance of the structure $3G_0$. Similar calculations carried out for silicon triangle+buckled hexagon+staggered triangle+buckled hexagon structure (Si_{H6}) have resulted in instable structure.

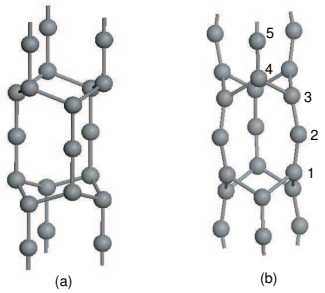

Figure 4.42: (a) Initial triangle+hexagon+staggered triangle+hexagon structure (C_{H6} and Si_{H6}). (b) The optimized structure of C_{H6} with $E_{binding} = 7.93eV$ and bond lengths $d_{12} = 1.319$Å, $d_{23} = 1.319$Å, $d_{34} = 1.52$Å, $d_{45} = 1.315$Å.

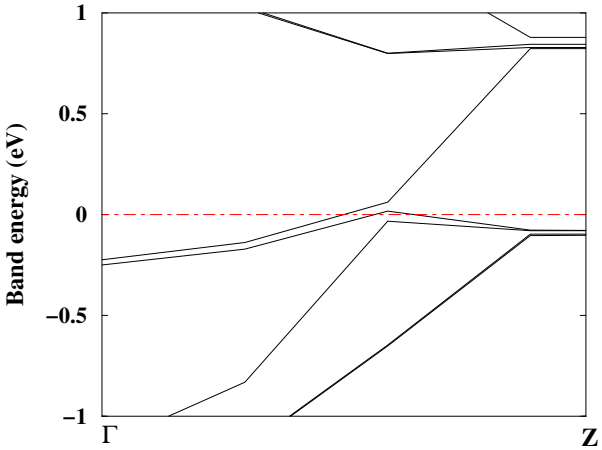

Figure 4.43: (a) Energy band structure of stable C_{H6} structure. There are roughly 3 bands that intersect Fermi level.

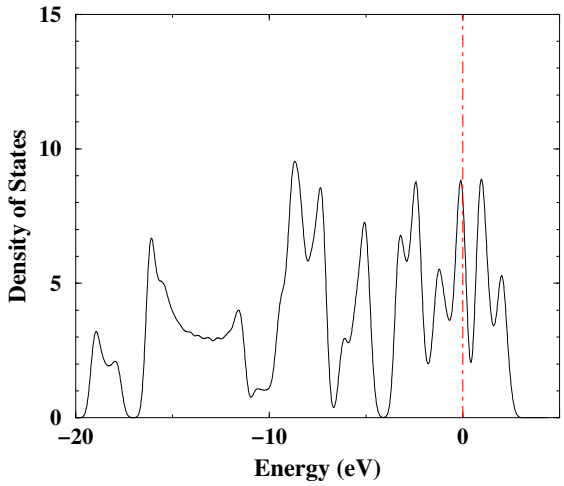

Figure 4.44: Calculated DOS of stable C_{H6} structure.

4.3.14 Silicon Nanotubes

Tubes are another class of structure for one-dimensional nanowires. In the past decade several novel properties of carbon nanotubes have been investigated actively. These properties have been used to make prototypes of various nanoscale electronic devices. In this thesis, we do not involve with the physical properties of carbon nanotubes. On the other hand Si being in the same IV column as C atom, has similar crystal structure. It is of intent to know whether Si has stable tubular structures.

Silicon (8,0) nanotubes is optimized by using 7 **k**-points and 300 eV energy cutoff value with supercell lattice parameters $a_s = b_s = 20$ Åand $c_s = c = 6.67$ Å. Optimization carried out by CG on the (8,0) tube yields binding energy $E_{binding} =$ 4.80 eV/atom ($E_{total} = -3455.88eV$). The relaxed structure is illustrated in Fig. 4.45.

Electrical properties of relaxed (8,0) tube are investigated by analyzing the calculated energy band structure in Fig. 4.46. We found silicon zigzag (8,0) tube is metallic with $G = 3G_0$ due to three bands intersecting the Fermi level.

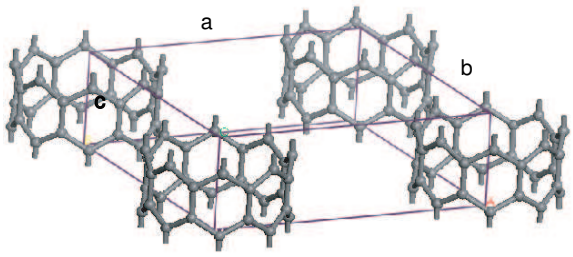

Figure 4.45: Silicon (8,0) tube in a supercell with lattice parameters $a_s = b_s =$ 20 Åand $c_s = 6$ Å. After optimization (8,0) tube relaxed to (8,0) tube with c=6.67Åand binding energy $E_{binding} = 4.80$ eV/atom.

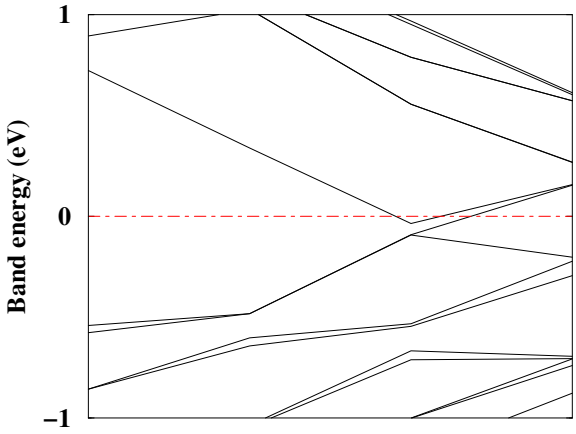

Figure 4.46: Energy band structure of silicon (8,0) tube. There are three bands intersecting the Fermi level.

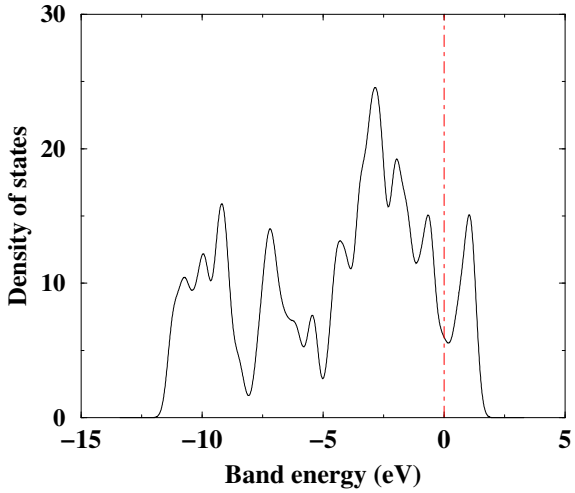

Figure 4.47: Calculated DOS of the silicon zigzag (8,0) SWNT. There is finite density of states at Fermi level represented by dashed dotted lines.

After obtaining the relaxed structure of the zigzag (8,0) Si tube, we performed stability test for this structure first by deforming it with a %20 strain. Upon relaxation, the strained (or deformed) tube did not returned to the initial (unstrained) structure.

This calculation reveals that silicon tubes are not stable as carbon nanotubes, since strained silicon tube does not return to its undeformed structure. But it is interesting that silicon tube neither relaxes to undeformed structure nor disintegrates. Other important result is that, relaxed deformed tube is energically more favorable than the relaxed structure of non-strained silicon (8,0) tube. This energy difference can be explained by the increased Si-Si interaction at the high curvature sites of the elliptically deformed tube. As far the electrical properties of metallic %20 strained structure are similar to the undeformed one, with $3G_0$ conductance value near Fermi level where $G_0 = 2e^2/h$.

After obtaining the general properties of silicon (8,0) tube, we focussed on (3,3) tube. By performing the similar calculations for armchair **Si (3,3) nanotube**, we obtained that the structure in Fig. 4.48 is stable with lattice parameter c=3.82Åand binding energy $E_{binding}$ = 4.7 eV/atom (E_{total} =

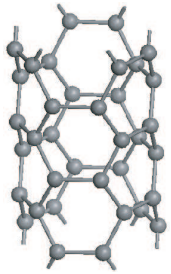

Figure 4.48: Relaxed structure of armchair silicon (3,3) nanotube. with c=3.82Åand binding energy $E_{binding} = 4.7$ eV/atom.

$-1294.66eV$).

By analyzing Band structure of silicon (3,3) tube, we concluded that the relaxed structure is metallic with $2G_0$ conductance.

We performed stability tests for silicon (3,3) tube, by deforming the structure in radial direction by amount of %5,%10 and %15. After relaxation, we observed that these structures return to the %5,%10 and %15 strained structures with total energies $E_{total_5} = -1294.61eV$, $E_{total_10} = -1294.60eV$ and $E_{total_15} = -1294.54eV$. By analyzing these energy values, we concluded that the non-strained silicon (3,3) tube is the most stable structure, but it should be noted that there is not much energy difference between these strained tubes.

Electrical properties of these structures are similar to that of silicon (3,3) tube, except that %15 strained (3,3) tube has $3G_0$ conductance value instead of $2G_0$ for other structures.

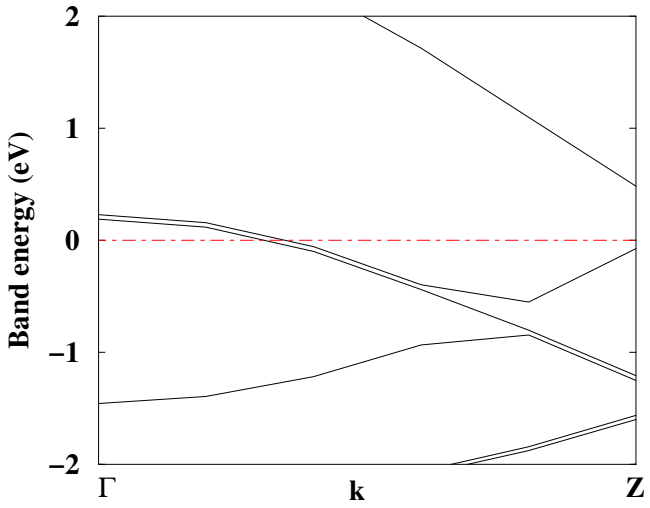

Figure 4.49: Calculated band structure of Si (3,3) nanotube. Two bands intersecting the E_F attribute metallic charecter to the structure.

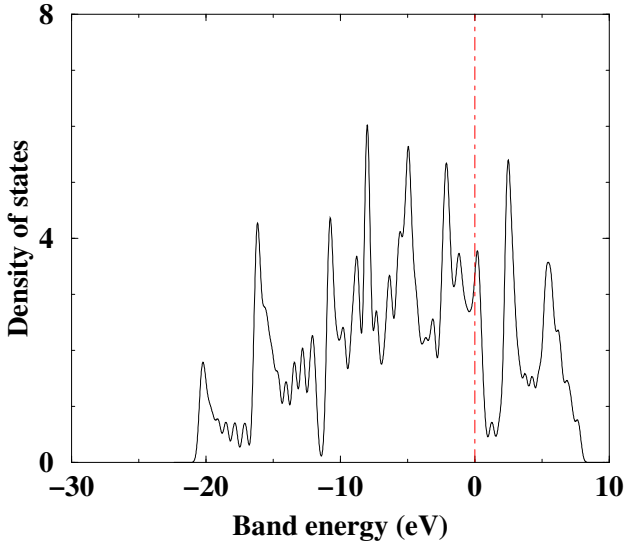

Figure 4.50: Calculated density of states of (3,3) armchair Si nanotube.

4.4 Conclusions and Future Work

4.4.1 Conclusions

Our work reveals a number of interesting physical properties of different types of silicon and carbon nanowires which are explained in the previous chapter. We believe that these findings are essential for future development of nanoelectronics design both experimentally and theoretically. The structures by themselves are important and essential to understand 1-D periodicity, namely crystallography in one-dimension. Now, we highlight some of the important findings by way of conclusion:

1. Carbon linear chain structure is the most stable structure among other stable carbon nanowires with binding energy $E_{binding} = 8.29eV/atom$ which is comparable with the cohesive energy of bulk carbon in diamond structure with $E_{binding} \simeq 8.43eV$ (Fig. 4.51).

The stability of the carbon chain atoms stems from the two-fold π-bonds formed by carbon $2p_x$ and $2p_y$ orbitals, and also σ-bond made from carbon 2s+$2p_z$ orbitals. As compared to the tetrahedrally bonded diamond, bonds in the linear chain are stronger and charge is more localized along the C-C bands. We specify the bond as double bond. This explains also why the cohesive energy of the carbon linear chain is comparable to the bulk diamond, in spite of the reduced nearest neighbor interaction (2 in chain, 4 in diamond) Interestingly, other structures, such as C2, C3 and C4, have changed to linear structure upon relaxation. In spite of the fact that diamond is an insulator with band gap ∼5.4 eV, the chain structure is metallic with quantum ballistic conductance G=$2G_0$. It is interesting to note that the conductance of carbon linear chain is twice larger than that of the gold linear chain.

Carbon linear chains have been fabricated in the center of carbon multiwall nanotubes (MWNT). The high stability of the carbon linear chain revealed in this thesis suggest that one can also obtain stable suspended carbon linear chains. One contemplates that stretching of SWNTs can give rise to linear chains.

We found that Si also form stable linear chain structure which exhibits physical properties similar to that of the carbon linear chain. It is metallic and has quantum ballistic conductance of $2G_0$. Si linear chains have not been synthesized yet. This work indicates that the fabrication of double bonded Si linear chain can lead to important applications, in particular as a interconnects in the Si-based microelectronics where device size is rapidly reducing to 20-30 nanometers.

Simple nanowire structures, which are similar to linear chain are zigzag and triangular structures can be formed by Si, but these structures are not stable in carbon. It has been shown that these structures are stable also in metals such as Al and Au. The instability of these structures in carbon are attributed to the absence of sizeable core electron density. We found that Si nanowires having triangular or zigzag structure are good conductors.

3. Some of the carbon nanowires from C_{T1} to C_{H6} has been disintegrated after optimization while others give stable structure with binding energy less than that of linear chain (C1). But it should be noted that, binding energy of C_{H5} and C_{H6} is still close to the bulk carbon binding energy and these structures are metallic.

4. None of the silicon nanowires has been disintegrated after optimization by using first-principle pseudopotential. Hence, we concluded that silicon element is possibly very suitable material for interconnection.

5. As described in detail in the previous section, we revealed a number of interesting nanowire structures; some of them stable in Si, some of them in C or in both elements. Some structures are metal, some are semiconductor. This work is opening a new field which is full of novel physical properties.

4.4.2 Future Work

Our more systematic study of stability using temperature dependent quantum molecular dynamics (QMD) and calculation of phonon spectrum is in progress. In fact, stability of the structure, such as linear chain have been tested by QMD and phonon density calculations.

We also performed first-principle calculations of transmission coefficient based on the Keldysh non-equilibrium quantum statistical mechanics. We plan to perform similar calculation for wires suspended between two electrodes.

We plan to extend our study for composite wires made by metal and Si (C) atoms, and calculate their magnetic properties. The magnetic ground state of these wires can be important for spintronics.

4.4.3 General Remarks

Based on the first-principles pseudopotential plane wave calculations, we showed that most of the Si and C based nanowires are metallic despite their parent bulk crystals are semiconductor or insulator and strongly directed bonds. In fact, Si and C being group IV elements have $(ns)^2$ and $(np)^2$ valance structure. One of the valance s-orbitals are promoted to p-state, and finally $(ns)^1$ $(np)^3$ valance orbital form four tetrahedrally directed $(sp)^3$ orbitals. These hybrid orbitals, in turn, form covalent bonds with nearest neighbor atoms. The crystal structure which is formed at the end is specified as diamond structure; it is an open structure but relatively strong owing to these directed bonds. Since number of electrons stored to each band are even, and also conduction bands do not overlap with the valance band, a finite band gap (1.1 eV for Si and 5.4 eV for diamond) forms between them. In nanowires, one faces a different situation, where the banding may be different from the tetrahedral coordination as far as number of bands and their directions are concerned. In the case of linear chain, each atom has two nearest neighbors and cylindrical symmetry. Then the atomic orbitals are forced to form double bands. Because of the cylindrical symmetry around the axis of the chain and valency of the atoms, the chain is metallic, and has conductance two times higher than the conductance of gold chain. The situation may be different for the nanowires which have coordination number higher that four. For certain pentagonal and hexagonal structures the number of nearest neighbor can be much larger than four, where the character of the bonds is remarkably different. As far the question, whether the bonding can be stable in spite of thee higher coordination can be sought in the 3D crystal structure of these elements

having different lattice's. In Fig. 4.51 and Fig. 4.52, we present the variation of interaction energy of C in bcc, fcc and diamond structures, having 8, 12 and four nearest-neighbors. It is seen that all three yields an attractive interaction with a cohesive energy at well defined lattice parameters. Of course, the highest binding and hence the global minimum occurs in the diamond structure. As demonstrated, structures yielding coordination numbers higher than four can result in a minimum on the Born-Oppenheimer surface.

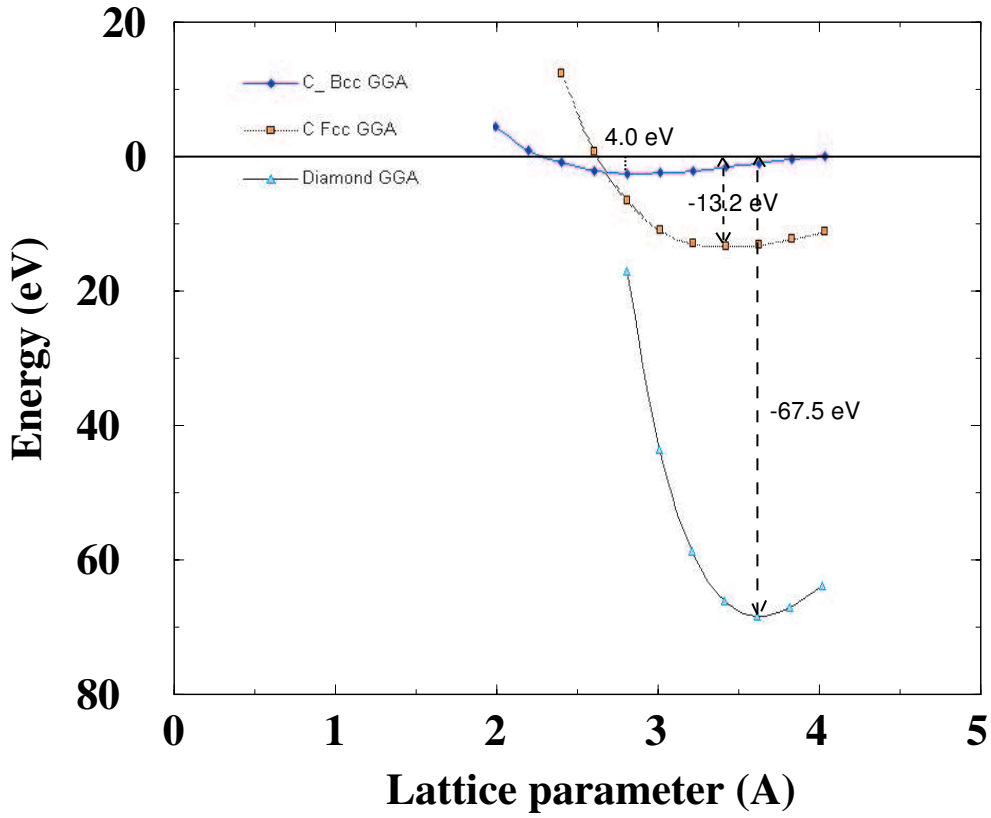

Figure 4.51: The variation of interaction energy of C in bcc, fcc and diamond structures obtained by using GGA. These structures have binding energies, $E_{bccbinding}$=-2 eV/atom, $E_{fccbinding}$=-3.3 eV/atom and $E_{diamondbinding}$=-8.43 eV/atom.

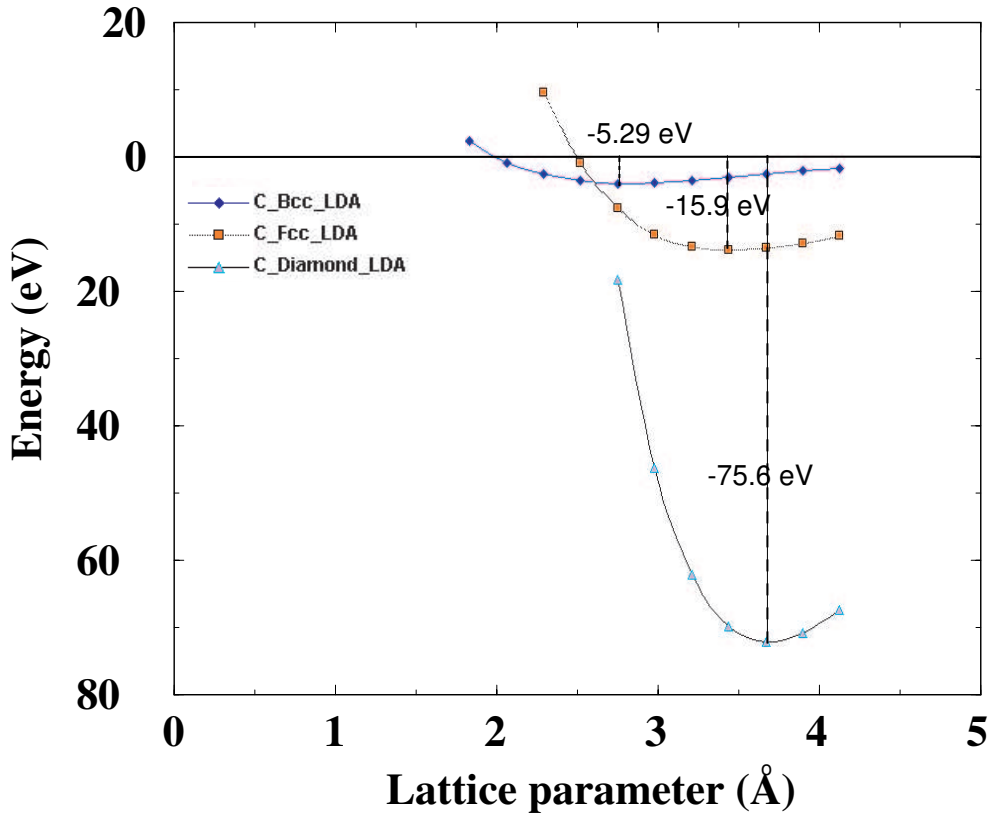

Figure 4.52: The variation of interaction energy of C in bcc, fcc and diamond structures with binding energies, $E_{bccbinding} = -2.64$ eV/atom, $E_{fccbinding} = -3.97$ eV/atom and $E_{diamondbinding} = -9.45$ eV/atom obtained by using LDA.

Bibliography

Bibliography

[1] H. Ohnishi, Y.Kondo and KK.Takayanagi, Nature 395,780 (1998)

[2] A.I.Yanson, G.R Bolliger, H.E. Van der Brom, N.Agrait and J.M. van Ruitenbeek, Nature 395,783 (1998)

[3] P.Sen, O.Gulseren, T.Yildirim, I.P.Batra and S.Ciraci Phys Rev. B 64, 195420 (2001)

[4] S. Iijima, Nature 354, 56 (1991)

[5] D. S. Bethune, C. H. Kiang, M. S. de Vries, G. Gorman, R. Savoy, J. Vazquez and R. Beyers, Nature 363, 605 (1993).

[6] S. Iijima and T. Ichihashi, Nature 363, 603 (1993).

[7] A. Thess, R. Lee, P. Nikolaev, H. Dai, P. Petit, J. Robert, C. Xu, Y. H. Lee, S. G. Kim, A. G. Rinzler, D. T. Colbert, G. E. Scuseria, D.Tomanek, J. E. Fischer, and R. E. Smalley, Science 273, 483 (1996).

[8] G.Dresselhaus, Ph.Avouris; Carbon Nanotubes Springer (2001)

[9] E.Durgun, S.Dağ ,S.Ciraci and O.Gulseren Journal of Physical Chem. (To be published) (2003)

[10] S.Dağ, E.Durgun and S.Ciraci Phys. Rev.B, Rapid Com. To be Published (2003)

[11] Stefan Frank et al., Science 280 1744 (1998)

[12] Hyoung Joon Choi,Jisoon Ihm,Young-Gui Yoon and Steven G. Louie Physical Review B Volume 60, 14009 (1999)

[13] Mehrez H, Ciraci S, Buldum A and Batra I P 1997 Phys. Rev. B 55 R1981

[14] Scheer E et al 1998 Nature 394 154

[15] Lang N D 1997 Phys. Rev. Lett. 79 1357

[16] Kalmeyer V R and Laughlin R B 1987 Phys. Rev. B 35 9805

[17] Yanson A I, Bolliger G R, van der Brom H E, Agrat N and van Ruitenbeek J M 1998 Nature 395 783

[18] Lang N D 1995 Phys. Rev. B 52 5335

[19] A.Buldum, S.Ciraci and C.Y.Fong J.Phys:Conds.Matter 12 3349-3358 (2000)

[20] Ozpineci A and Ciraci S 2001 Phys. Rev. B 63 125415

[21] M.Born and J.R Oppenheimer, Ann der Phys. 84,457 (1927)

[22] D.R.Hartree, Proc. Cambridge. Philos.Soc. 24, 89 (1928)

[23] V.Forc, Z.Phys. 61,126 (1930)

[24] J.C.Slater,Phys. 35, 210 (1930)

[25] L.H. Thomas, Proc. Cambridge. Philos.Soc. 24, 89 (1928)

[26] E.Fermi, Z.Phys. 48,73 (1928)

[27] P.Hohenberg and W.Kohn, Phys.Rev 136.B864 (1964)

[28] W.Kohn and L.J.Sham, Phys.Rev. 140,a1133 (1965)

[29] James C. Phillips Phys.Rev. 112 3, 685 (November 1958).

[30] James C. Phillips and Leonard Kleinman. Phys. Rev. 116 2, 287 (1959).

[31] Charles Kittel, Introduction to Solid State Physics, 7th edition

[32] J. Ihm. Rep. Prog. Phys. 51 (1), 105 (1988).

[33] W. E. Pickett. Comp.Phys. Rep. 9 (3), 115 (1989).

[34] P.Fulde Electron Correlations in Molecules and Solids Springer-Verlag,Berlin.(1993)

[35] J.Perdew Intl. J. Quant. Chem 57 309 (1996)

[36] D. R. Hamann Phys. Rev. Lett. 76 660 (1996)

[37] R.Landauer, Philos. Mag. 21, 863 (1970)

[38] S. Datta, Electronic Transport in Mesoscopic Systems Cambridge University Press, Cambridge, (1995)

[39] M.B.Nardelli Phys Rev.B Vol.60 7828

[40] Slater, Koster Phys. Rev B. Vol.17 2376

[41] W.A.Harrison, Electronic Structure and Properties of Solids, Freenman, San Fransisco (1980)

[42] Phillips, Pandey Phys. Rev.B, 13, 750 (1976)

[43] C.H.Xu, C.Z.Wang, C.T. Chan and K.M.Ho Journal of Phys Cond. Matter, Vol 4, 6047 (1992)

[44] N.W.Ashcroft, N.D.Mermin Solid State Physics, Sounders College Publishing (1970)

[45] J.P.Perdew, J.A.Chevary, S.H.Vosko, K.A.Jackson, M.R.Pederson, D.J.Singh and C.Fiolhois, Phys Rev.B **46**, 6671 (1992)

[46] D.Vanderbilt, Phys. Rev. B **41**, 7892 (1990)

[47] H.J.Monkhorst and J.D.Pack, Phys. Rev.B. **13**,5188 (1976)